

AUS Repository

Modeling of Chlorophyll-a and Eutrophication Indicators in the Dubai Creek Area using Remote Sensing

Item Type	Thesis
Authors	Bachir, Abdallah Raafat
Download date	2026-06-08 03:11:29
Link to Item	http://hdl.handle.net/11073/7773

MODELING OF CHLOROPHYLL-A AND EUTROPHICATION INDICATORS IN THE
DUBAI CREEK AREA USING REMOTE SENSING

By

Abdallah Raafat Bachir

A Thesis Presented to the Faculty of the
American University of Sharjah
College of Engineering
in Partial Fulfillment
of the Requirements
for the Degree of
Master of Science in
Civil Engineering

Sharjah, United Arab Emirates

January 2015

Approval Signatures

We, the undersigned, approve the Master's Thesis of Abdallah Raafat Bachir.

Thesis Title: Modeling of Chlorophyll-a and Eutrophication Indicators in the Dubai Creek Area using Remote Sensing

Signature

Date of Signature

(dd/mm/yyyy)

Dr. Md. Maruf Mortula
Associate Professor, Department of Civil Engineering
Thesis Advisor

Dr. Tarig Ali
Associate Professor, Department of Civil Engineering
Thesis Co-advisor

Dr. Serter Atabay
Associate Professor, Department of Civil Engineering
Thesis Committee Member

Dr. Varkki Pallathucheril
Professor, College of Architecture, Art and Design
Thesis Committee Member

Dr. Ali Akan
Head, Department of Civil Engineering

Dr. Mohamed El Tarhuni
Associate Dean, College of Engineering

Dr. Leland Blank
Dean, College of Engineering

Dr. Khaled Assaleh
Director of Graduate Studies

Acknowledgements

I would like to express my deepest gratitude toward my supervisors, committee members, and my family members. Completion of this research wouldn't have been possible without them. I would like to thank Dr. Maruf Mortula and Dr. Tarig Ali for believing in my abilities, for helping me overcome the various problems faced during this research, and for motivating me for around two years. I would like to thank my committee members, Dr. Serter Atabay and Dr. Varkki Pallathucheril for their supportive comments and discussions. I would also like to express, from the bottom of my heart, my deepest appreciation and enormous love for my family members, especially my father and my mother. Their support, care, and love toward me during my whole life were without limits. Reaching what I have reached at this point of my life wouldn't have been possible without them. Finally, I would like also to thank my two sisters for all the support and encouragement I received from them during the past years which helped me achieve my goals in life so far. For all the people mentioned above and to everyone else I know, I really appreciate that you are part of my life.

Dedicated to my family.

Abstract

The last few decades have witnessed an increase in the frequency and magnitude of the occurrences of algal blooms in coastal regions. A high increase in the levels of nutrients (phosphorus and nitrogen) in the water column leads to excessive algal growth, known as eutrophication. The presence of a large amount of algae normally turns water green or red in the case of Harmful Algal Blooms (HABs). Chlorophyll-a is the main indicator of algal blooms and its concentrations are used as indicators of the scale of an algal bloom. Nutrients have a major impact over algal blooms. Dubai Creek is a salt water body located in Dubai, UAE which divides the city into Bur Dubai and Deira. Due to high levels of human activities surrounding the creek, there have always been eutrophication concerns given the levels of nutrients in the creek. In the last few years, remote sensing algorithms have been developed to monitor algae in water bodies by mapping chlorophyll-a concentrations. The aim of this study was to map chlorophyll-a in the Dubai Creek from WorldView-2 imagery (high resolution satellite images) and to explore the relationship between chlorophyll-a and other eutrophication indicators. A geometrically and atmospherically corrected Worldview-2 image and in-situ data have been utilized to map chlorophyll-a in the creek. A spectral model was developed to retrieve chlorophyll-a concentrations from the WorldView-2 multispectral image. The model showed an R-squared value of 0.82 with in-situ chlorophyll-a data. Another model was developed for the relationship between the levels of spectral chlorophyll-a and total nitrogen and phosphates, which showed an R-squared value of 0.97. The developed models are to be used in the mapping of chlorophyll-a, total nitrogen, and phosphates without the need for expensive in-situ monitoring efforts since they will provide values of these parameters everywhere in the creek.

Search Terms: Algal blooms, Chlorophyll-a, Dubai Creek, Nutrients, Remote sensing,

Table of Contents

	Page
Abstract	6
List of Tables	10
List of Figures	12
1 Introduction	14
1.1 Background Information	14
1.2 Problem Statement	14
1.3 Objectives	15
2 Literature Review	16
2.1 Water Quality Modeling	16
2.2 Algal Blooms	16
2.2.1 Known Algal Bloom Incidents	17
2.3 Remote Sensing	18
2.3.1 Image Pre-Processing	19
2.3.1.1 Atmospheric Correction	20
2.3.2 Satellite Resolution	20
2.4 Chlorophyll-a Retrieval Algorithms	22
2.4.1 Analytical Algorithms	23
2.4.2 Empirical Algorithms	23
2.4.2.1 Narrow-Band Algorithms	24
2.4.2.2 Broad-Band Algorithms	25
2.5 Eutrophication Indicators	26

3 Materials and Methodology	29
3.1 Materials	29
3.1.1 Satellite Image	29
3.1.2 In-Situ Data	29
3.2 Methodologies	30
3.2.1 Image Pre-Processing	30
3.2.1.1 Geometric Correction	30
3.2.1.2 Radiometric Correction	33
3.2.1.3 Atmospheric Correction	34
3.2.2 Chlorophyll-a Spectral Modeling	37
3.2.3 Modeling the Relation between Chlorophyll-a and Eutrophication Indicators	38
3.2.4 Modeling Spectral Characteristics of Water Columns with Their Content of Eutrophication Indicators	39
3.3 Study Limitations	39
4 Results and Discussion	41
4.1 Data Preparation and Image Preprocessing	41
4.2 Spectral Chlorophyll-a Modeling	43
4.3 Empirical Relation between Chlorophyll-a and Eutrophication Indicators	51
4.4 Correlation between Spectral Chlorophyll-a and Eutrophication Indicators	56
5 Conclusions and Future Work	62
5.1 Conclusions	62
5.2 Future Work	62

References	63
Appendix A: Earth-Sun Distance Calculation	67
Appendix B: Solar Zenith Angle Calculation	68
Appendix C: Conversion from Digital Numbers to Top-of-Atmosphere Radiance to Ground-Leaving Reflectance	68
VITA	72

List of Tables

	Page
Table 1: Outcomes of interaction of electromagnetic energy with matter	18
Table 2: Examples of common applications of remote sensing	19
Table 3: Comparison of spatial, spectral, temporal, and radiometric resolutions of Satellites highly utilized for ocean color studies	22
Table 4: Summary of chlorophyll-a models developed in different studies for use with broad-band satellites imagery	27
Table 5: Water quality data - Quarter 2, 2012	31
Table 6: Water quality data - Quarter 3, 2012	32
Table 7: DLTM projection parameters	33
Table 8: Absolute radiometric calibration factor and effective bandwidth for each of WorldView-2 bands	34
Table 9: Band-averaged solar spectral irradiance values for WorldView-2 bands	35
Table 10: Quarterly and interpolated chlorophyll-a values	41
Table 11: DN and radiance values of haze selected for the COST atmospheric correction method	42
Table 12: WorldView-2 bands description	44
Table 13: Best performing models along with their R-squared values	47
Table 14: Field and spectral differences of chlorophyll-a values	48
Table 15: Annual change in measured chlorophyll-a concentrations	49
Table 16: Comparison between field and modelled TN/P values	57
Table 17: Summarization of the modelling steps	58

Table 18: Spectral TN/P and corresponding spectral chlorophyll-a values	60
Table A.1: Digital numbers corresponding to stations locations	68
Table A.2: Top-of-atmosphere radiance corresponding to stations locations	69
Table A.3: Ground-leaving reflectance corresponding to stations locations	69
Table A.4: Randomly selected DN values and their conversion parameters	70
Table A.5: Randomly selected radiance values and their conversion parameters	70

List of Figures

	Page
Figure 1: Empirical algorithm for mapping of chlorophyll-a	24
Figure 2: Reflectance spectra of chlorophyll-a	25
Figure 3: The extents of the WorldView-2 imagery showing the Dubai Creek and the water quality monitoring stations	29
Figure 4: Model created in ERDAS Imagine to convert DNs to radiance	35
Figure 5: COST model developed for ERDAS Imagine to perform the atmospheric correction	37
Figure 6: Spectral chlorophyll-a map generation using ERDAS Imagine 2011	38
Figure 7: Eutrophication indicators map generation using ERDAS Imagine 2011	39
Figure 8: A flow chart summarizing the steps used in this study	40
Figure 9: Band 1 (coastal blue) DN of haze selection	43
Figure 10: Correlation between the field and spectral chlorophyll-a values (C+NIR1)/NIR2	44
Figure 11: Correlation between the field and spectral chlorophyll-a values (B+NIR1)/NIR2	45
Figure 12: Correlation between the field and spectral chlorophyll-a values (G+NIR1)/NIR2	45
Figure 13: Correlation between the field and spectral chlorophyll-a values (Y+NIR1)/NIR2	46
Figure 14: Correlation between field and spectral chlorophyll-a values (B+NIR1)/RE	46
Figure 15: Spectral chlorophyll-a map	50

Figure 16: Correlation between eutrophication indicators and field chlorophyll-a (TN/P)	52
Figure 17: Correlation between eutrophication indicators and chlorophyll-a (salinity)	53
Figure 18: Correlation between eutrophication indicators and field chlorophyll-a (P/salinity)	53
Figure 19: Correlation between eutrophication indicators and field chlorophyll-a (Phosphates)	54
Figure 20: Correlation between eutrophication indicators and field chlorophyll-a (TN/salinity)	54
Figure 21: Correlation between field and modeled TN-P ratio	55
Figure 22: Dubai Creek TN/P map	59
Figure 23: Correlation between spectral chlorophyll-a and field TN/P	60
Figure 24: Correlation between spectral and field TN-P ratios	61

1 INTRODUCTION

1.1 Background

Water bodies have been polluted from different sources in the last few decades, affecting the aquatic life in many ways which in turn may directly or indirectly affect the health of human beings. These sources include oil spills, garbage dumping, discharging of untreated or partially treated wastewater, toxic wastes, algal blooms, and many others.

Remotely-sensed imagery has been utilized by researchers to study water quality, hazards and sources of pollution easily and accurately. The presence of algae in water bodies is expected; however, the increase of its concentrations is a source of concern since it acts as an isolating layer that reduces dissolved oxygen concentrations in water bodies [1]. Chlorophyll-a is the green or reddish green pigment found in all plants and is the main indicator of the presence of algae. Other factors that influence algal growth besides nutrients include sunlight and temperature [2]. The coasts of the United Arab Emirates, including that of Dubai, were affected by the catastrophic Harmful Algal Bloom (HAB), commonly known as the red tide in 2008 and 2009. The event, which lasted for a few months over the two years, caused massive fish kills and forced the closure of many beaches [3]. This event emphasized the necessity of research in this area. One study utilized a combination of remote sensing images and in-situ data to perform a multiple linear regression to map chlorophyll-a concentrations along Dubai Creek [4]. Another one attempted mapping of chlorophyll-a concentrations utilizing satellite imagery and a hybrid coordinate ocean numerical model [5]. However, mapping of chlorophyll-a throughout the creek using high resolution satellite imagery was missing.

1.2 Problem Statement

There have been increases in the frequencies of algal bloom occurrences and magnitudes in the region, mostly caused by anthropogenic factors. The current in-situ methods for monitoring algae are point based and insufficient due to the high cost associated with them. Therefore, remote sensing algorithms have been developed in recent years to monitor algae in water bodies. These algorithms are mostly time- and

site-specific, as they are not applicable to different locations or periods of time [6]. Therefore, in order to monitor eutrophication of the creek, new models are needed.

1.3 Objectives

The overall objective of this study is to model the spatial distribution of chlorophyll-a and eutrophication indicators in the Dubai Creek. The specific objectives are

- To develop a model with high resolution WorldView-2 satellite imagery and field chlorophyll-a data of Dubai Creek.
- To develop another model using the same imagery that relates chlorophyll-a and eutrophication indicators in Dubai Creek.

The major steps to achieve this objective include image pre-processing and atmospheric correction, spectral band ratio model development and calibration and spectral chlorophyll-a and eutrophication indicators modeling and calibration.

2 Literature Review

2.1 Water Quality Modeling

Water quality modeling is the process of estimating the levels of pollution in water and assessing the impact of the environment on the process [7]. Water quality models can be analytical or empirical. Analytical models utilize scientific facts and field observations to represent water quality parameters, while empirical models use statistical methods to correlate measured and other observed parameters. Water quality modeling can be carried out for both point and nonpoint source pollution. Point source pollution normally results from a known location in space such as the discharge point of a treatment plant that discharges untreated waste. Nonpoint source pollution results from an activity over an area such as fertilizers surface runoffs resulting from agricultural activities. Point sources are easier to measure, model and control compared to nonpoint sources [8].

2.2 Algal Blooms

An algal bloom is an algal population which has exceeded a certain limit in a certain area of a water body. Algal blooms are classified into harmful and non-harmful, while algae are divided into autotrophic or heterotrophic organisms [9]. Autotrophic organisms use inorganic raw material to get energy and form organic molecules, while heterotrophic ones get their food from other organisms. Algae fall under the phytoplankton category along with cyanobacteria. Phytoplankton are defined as the microscopic organisms that live in both salty and fresh water.

Phytoplankton blooms have increased both in frequency and size in recent years. One main cause of algal blooms is the increase in nutrient concentrations. An increase in nutrient concentrations can be caused by coastal upwelling or other natural causes such as certain temperature and light availability [10, 11]. Scientific evidence suggests that the main reason for the increase of nutrients, mainly total nitrogen and total phosphorus, in water bodies is the increase in the agricultural and industrial activities driven by the increase of the Earth's population [12].

An excess amount of nutrients in water causes massive algal growth. The dead algae will accumulate on the bottom of the water body and will be consumed by bacteria. Depending on environmental factors, the levels of dissolved oxygen will

decrease as it gets consumed by bacteria. This process results in a possible death of fish and shellfish [7]. Usually, there is more than one nutrient in water at varying concentrations. Accordingly, there is always a nutrient that limits the growth of phytoplankton which is commonly called the “limiting nutrient”. Identification of the limiting nutrient can be done through laboratory testing. In this test, if increasing a nutrient results in an increase in cellular growth of algae, then this nutrient is the limiting nutrient. In most water bodies around the world, the total phosphorus is the limiting nutrient since total phosphorus concentrations are hugely affected by anthropogenic activities [13]. Also, scientific evidence suggests that in estuaries, the limiting nutrient is mostly seasonal-based; for example, the limiting nutrient can be nitrogen in summer and phosphorus in winter [14]. Another factor that plays an important role in the increase of algae is the concentrations of total suspended matter [15].

The main indication that is used to monitor algal blooms is the chlorophyll-a levels. Chlorophyll has many different types that are well known. However, the type of interest in this study is chlorophyll-a that is found in algae organisms [10]. So, algal blooms can be detected using remote sensing techniques by monitoring chlorophyll-a levels in water.

2.2.1 Known Algal Bloom Incidents

There have been many harmful algal bloom incidents around the world in the last few decades. One that is recent and important to the region of the Arabian Gulf occurred in August 2008 and lasted for more than eight months. This was a bloom of dinoflagellate *Cochlodinium polykrikoides* that occurred in the Arabian Gulf and Gulf of Oman resulting in massive fish kills, restriction of fishing, and many problems in desalination plants [3]. Initial studies suggested that the gene sequences of this type of algae were similar to the ones found in HABs that hit American coasts, but was different than those found in other places. It was also concluded that these types of blooms are likely to happen in the future in the region [3].

Another famous incident is one that happened in Korean waters in 1995. This incident caused massive fish kills and financial losses approximated around 95 million US dollars [16]. Another known incident of algal blooms includes the one that

occurred on the shores of Japan causing massive financial losses in the fish industry [17]. The American shores have been affected by blooms of many species including the almost annual blooms of *Karenia Brevis* along the west coast of Florida, the aforementioned dinoflagellate *Cochlodinium polykrikoides*, and other species such as dinoflagellate *Alexandrium fundyense* and *Alexandrium catanella* [18].

2.3 Remote Sensing

Remote sensing is the process of acquiring information about an object or a place on the ground without physical contact. The remote sensors are normally onboard a satellite or an aircraft [19].

Remote sensors are designed to detect electromagnetic energy at different wavelengths as they interact with matter through five possible processes: reflection, scattering, emission, absorption, and transmission, which are described in Table 1. Reflection is the most essential process of interaction with matter in remote sensing as the reflected electromagnetic energy at different wavelengths is used as inputs in various remote sensing algorithms.

Table 1: Outcomes of interaction of electromagnetic energy with matter [20]

Type of interaction	Description
Transmission	Radiation passes through matter
Absorption	Radiation transformed to mostly heat
Emission	The matter emits energy
Scatter	Radiation is scattered at different angles
Reflection	Radiation is reflected in any angle

There are many common applications of remote sensing, a few of which are shown in Table 2 [20]. Normally, a remote sensing image needs to be preprocessed by correcting for geometric, radiometric, and atmospheric errors before processing it to derive information about the objects of interest on the ground. The following paragraphs explain the typical preprocessing procedures of a remote sensing image as well as the processing of the corrected image to extract useful information about the

ground objects; in this case the imagery was used to estimate chlorophyll-a concentrations.

2.3.1 Image Pre-Processing

Pre-processing of remote sensing imagery involves geometric, radiometric, and atmospheric corrections. While the methods for applying the first two corrections are recognized globally, atmospheric correction remains a challenge in remote sensing [21]. Geometric corrections are

Table 2: Examples of common applications of remote sensing

Field of Application	Example
Agriculture	Condition assessment of crop
Forestry	Monitoring health of forests
Geology	Identifying mineral resources
Hydrology	Soil moisture content study
Sea Ice	Ice motion
Land use	Managing natural resources
Mapping	Mapping of elevations (contour)
Coastal Monitoring	Oil spill mapping

applied using Ground Control Points (GCP) in the area of the image to make sure that the location of each object on the image is an accurate representation of its real-world location [22]. Moreover, re-projection of images into the local coordinate system of the image area is a common procedure so that any other data available for the area can be represented in the same coordinate system. Radiometric correction removes sensor-related errors such as bad lines and strips and corrects for sun angle and topographic errors. This process is normally followed by conversion of the Digital Numbers (DN) in the image to error-free radiance values. The following subsection discusses atmospheric correction.

2.3.1.1 Atmospheric Correction

Although atmospheric correction is needed for almost any remote sensing applications, when mapping chlorophyll-a in water bodies, atmospheric correction is more challenging because the water-leaving reflectance is generally weak [21]. The atmosphere contributes to radiance values leaving the ground (“ground-leaving radiance”) in an additive or multiplicative form caused by atmospheric absorption or scattering. Therefore, radiance values detected by the sensor don’t represent ground-leaving radiance accurately. Many methods have been proposed since the 1990s to correct for atmospheric effects. In general, these can be divided into three categories: image-based, empirical line, and simulation methods.

The first category which is the image-based methods doesn’t require additional measurements and can be derived for any satellite image. One of the well-known image-based models is the Dark Object Subtraction (DOS). This method assumes that dark objects available in any scene should have a zero reflectance. However, due to the effects of the atmosphere the sensor records a value higher than zero for such objects. Therefore, the radiance value of that object should be subtracted from all pixels in that band. This method and the cosine of the sun zenith angle (COST) method [23] (an improvement of the DOS method) are still applied to these days and still produce successful results [24]. The COST method assumes that the reflectance value of the dark object is 1% instead of zero as very dark objects are rarely found in nature.

The second category is known as the empirical line method. This method starts by measuring reflectance values at selected points of a scene using a spectrometer, fitting these values with at-sensor radiance statistically, and using the statistical formula to estimate ground-leaving reflectance values in the whole image [25]. This method provided satisfactory results when used with IKONOS imagery [26]; therefore one would expect it to work just fine with high-resolution imagery.

The third category is the simulation methods which include the 6S and MODTRAN. Although these methods produce the most accurate results, their application is tedious as they require atmospheric data about the scene at the time of

acquisition to simulate the atmospheric effects [26]. Obtaining such information can be difficult and even impossible for old satellite images.

2.3.2 Satellite Resolution

Another important aspect to consider before initiating a remote sensing study is the selection of the imagery with the suitable resolution for the type of remote sensing application at hand. There are four types of resolutions, which are spatial, spectral, temporal, and radiometric resolution. Spatial resolution is related to the finest details that can be observed in the image. The spatial resolution can be described as the pixel size in ground units. Accordingly, the smaller the pixel size the higher the resolution of the image. Spectral resolution is related to the sensitivity of a sensor at a specific wavelength, and therefore it's the number of image bands detectable by a sensor and their corresponding wavelengths. Temporal resolution of a sensor is measured by the time it takes the sensor to complete an entire orbit cycle before it revisits the same area (aka revisit time), which is usually expressed in days. Radiometric resolution is defined as the possible degree of variation in a pixel value in any of the bands. For example, an 8-bit radiometric resolution of a sensor means that the sensor is capable of producing pixels that have values anywhere from 0 to 255 (i.e. 2^8-1). Table 3 shows the resolution of some common remote sensing satellites.

From Table 3, one would note the following:

- WorldView-2 has the highest spatial resolution among the listed satellites.
- The major difference between the satellites in this table is the number of bands when compared to the wavelength covered which divides them into narrow and broad band satellites.

Given the number of bands and the wavelength range, MODIS, MERIS, and SeaWiFS are considered narrow-band satellites. The average band width in these satellites mostly doesn't exceed 40nm and is averaged at around 20nm. Note that the center wavelength values of the bands of these satellites are chosen as to capture specific objects on earth.

Table 3: Comparison of spatial, spectral, temporal, and radiometric resolutions of satellites highly utilized for ocean colour studies

Satellite	Pixel size (m)	No. of bands	Wavelength covered (nm)	Revisit time (d)	Radiometric resolution	Reference
MODIS	250x250	19	405-965	1-2	12-bit	[27]
IKONOS	4x4	5	445-853	3	11-bit	[28]
SPOT	6x6	5	455-890	1	12-bit	[29]
SeaWiFS	1000x1000	8	402-885	1	10-bit	[30]
MERIS	260 or 1200	15	412.5-900	3	12-bit	[31]
LandSat 8	30x30	11	430-1380	16	12-bit	[32]
WorldView-2	2x2	9	400-1080	1.1	11-bit	[33]

Therefore, application of models that utilize reflectance at certain wavelengths is possible with such satellites. There are models developed specifically for some of these satellites such as the SeaWiFS OC4.v4 and MODIS OC3M which are used for ocean color studies. On the other hand, IKONOS, SPOT, and WorldView-2 are termed “broad-band” satellites. The bands in these satellites usually exceed 40nm and they are not centered at specific wavelengths on the contrary of narrow-band satellites. However, they have a much higher spatial resolution compared to the narrow-band satellites.

2.4 Chlorophyll-a Retrieval Algorithms

Chlorophyll-a retrieval algorithms can be divided into two main categories: (a) analytical (model-based) and (b) empirical. Each of the two categories has its principles, advantages, and disadvantages, which are detailed in the following subsections.

2.4.1 Analytical Algorithms

Analytical algorithms deal with remote sensing reflectance in terms of water inherent optical properties (IOPs) using “radiative transfer modelling” [6]. The analytical algorithm typically has forward and inverse processes. The forward process predicts water-leaving radiance by analyzing absorption and scattering characteristics of all the optical components of the water column. The inverse process predicts the levels of water constituents such as chlorophyll and total suspended solids (TSS) through the predicted water-leaving radiance [34]. One of the most known analytical algorithms is the MERIS Case II water algorithm. This algorithm utilizes the reflectance values of bands 1-7 and 9 and three angles (solar zenith, viewing zenith, and azimuth difference) of MERIS in order to estimate chlorophyll-a concentrations as well as total suspended matter and absorption of gelbstoff, which is a chromophoric component of dissolved organic matter [34]. In spite of the complexity of such models and the extensive measurements required to apply them, the results are not always satisfactory. The MERIS Case II water algorithm was found to underestimate reflectance values when checked against in-situ measurements, suggesting poor atmospheric correction results [35]. Scientific evidence suggests that poor results from such algorithms can be due to the additive nature of the IOPs and their use in estimating reflectance values [36].

Another type of algorithm that is classified into this category is the so-called semi-analytical algorithm. These algorithms use algebraic solutions to derive water parameters from the predicted water leaving radiance [6]. One of the best known semi-analytical algorithms is the “MODIS semi-analytical ocean color” algorithm. This algorithm estimates chlorophyll-a concentrations by utilizing the difference between measured sea-surface and nitrate-depletion temperatures to select a suitable chlorophyll absorption coefficient to estimate chlorophyll-a concentrations [37].

2.4.2 Empirical Algorithms

Empirical algorithms are simple to derive when compared to analytical algorithms. However, most empirical algorithms derived to estimate chlorophyll-a concentrations are time and site-specific. In other words, applying them in different locations or even at the same location at a different time may produce unsatisfactory results. Another

disadvantage of empirical algorithms is their inability to distinguish between signals of different parameters such as total suspended solids and chlorophyll-a [6]. Figure 1 illustrates the general approach followed when mapping chlorophyll-a concentrations using empirical algorithms. Empirical algorithms for mapping chlorophyll-a can be subdivided into algorithms that utilize narrow-band sensors and those that utilize broad-band sensors.

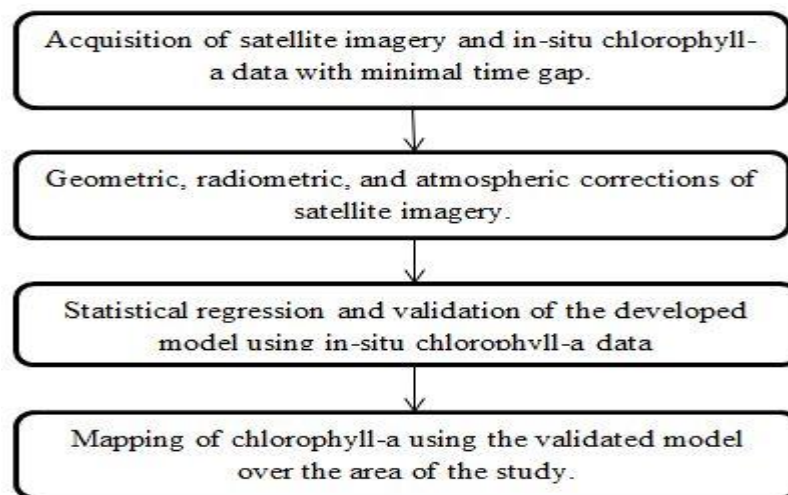


Figure 1: Empirical algorithm for mapping chlorophyll-a

2.4.2.1 Narrow-Band Algorithms

As the name implies, these types of algorithms are mostly applicable to satellite imagery with narrow bands (small wavelength ranges). Normally, these algorithms specify reflectance at a certain wavelength as an input of the model. Obtaining such values is normally not possible unless one of the bands is centered at that wavelength. An example of these algorithms is the Maximum Chlorophyll Index which is only applicable to MERIS imagery due to the use of the band centered at 708.75nm [2]. There are many studies on this topic, and they generally fall under one of the following points:

- (a) Blue/green band ratio

Chlorophyll-a is a green pigment that absorbs most of the blue and red light while reflecting most of the green light. The peak reflectance in the blue region is around

440nm while the peak of reflectance in the green region is around 530-550nm (Figure 2). It's important to note that reflectance spectra of chlorophyll-a in different regions doesn't have the exact same values of peak reflectance and peak absorption, though they are usually close [38]. Therefore, the use of a blue-to-green ratio can help in separating clear "blue" water columns from those rich in phytoplankton. However, the use of this ratio in case II waters where concentrations of Total Suspended Matter (TSS) and Colored Dissolved Organic Matter (CDOM) are high, does not provide highly correlated results due to the contribution of TSS and CDOM to the backscattering of light [39].

(b) Red/NIR band ratio

The absorption peak of chlorophyll-a is around 670nm and high absorption of water is around 700nm. The minimal effect of CDOM and TSS in the wavelength range 670-700nm region has allowed for better results in optically complex waters compared to the Blue/Green band ratio (Figure 2) [2].

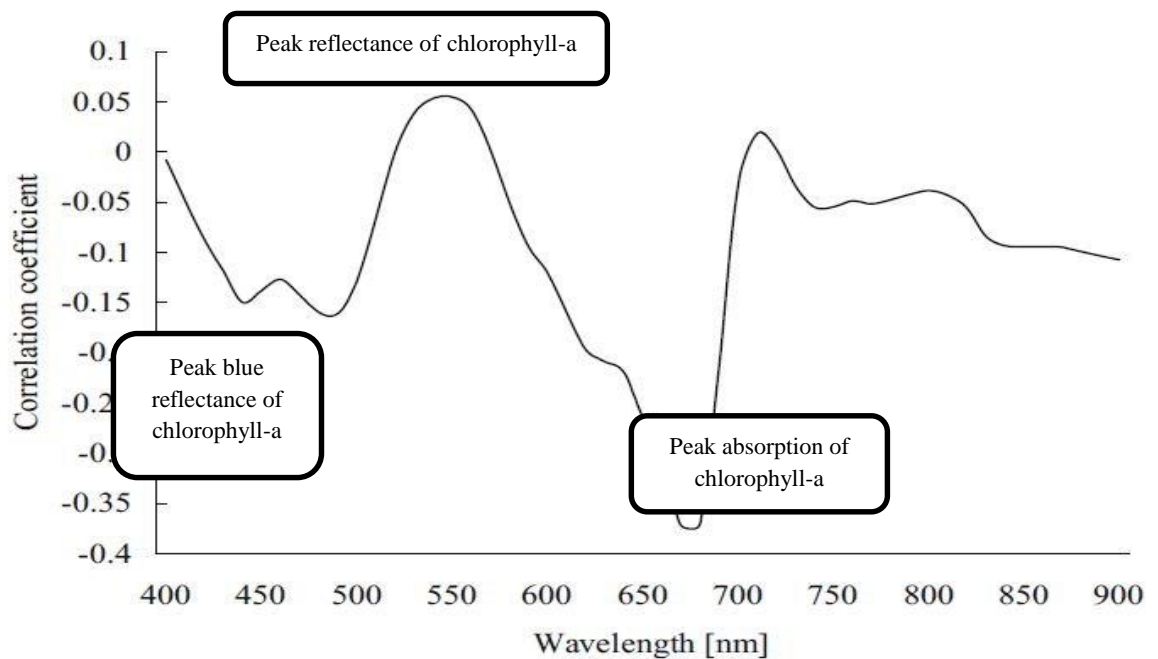


Figure 2: Reflectance spectra of chlorophyll-a

(c) Other algorithms

There have been other models proposed that fit the band center of some satellites but not others. Fluorescence Line Height (FLH) can't be applied to SeaWiFS satellite images due to the lack of bands in the wavelength range 670-690nm. The Floating Algae Index (FAI) algorithm subtracts the red edge and a linear "baseline" between red and short-wave infrared bands and is only applicable to MODIS [2].

2.4.2.2 Broad-Band Algorithms

Broad-band satellites such as SPOT, LandSat, IKONOS, and WorldView-2 don't have the focused bands of the narrow-band satellites and therefore the application of the algorithms mentioned earlier on their imagery is not possible. Current studies that utilize broad-band satellites use band-ratio methods and regression analysis to develop chlorophyll-a models and calibrate and evaluate them using the in-situ data. Table 4 summarizes some of the chlorophyll-a models developed in different studies for use with broad-band satellite imagery along with the coefficients of correlation with in-situ data. Also listed in Table 4 are the atmospheric correction methods used in each of these studies.

Some of these studies have obtained high correlations with chlorophyll-a in-situ data while others have not. However, most of these studies do not provide logical explanations and justifications of the development of their models. Research on the topic continues in order to develop new chlorophyll-a models that can provide a faithful representation of real-world values.

2.5 Eutrophication Indicators

Eutrophication is defined as the increase in the supply rate of organic matter (organic nutrients) in an ecosystem [44]. The availability of a supply of organic matter is not harmful by itself. However, the increase in this supply beyond a point where marine organisms are able to consume them is problematic. Organic matter will not be consumed completely and therefore it will accumulate and decay in the water system creating serious problems.

This increase in the supply of organic matter is caused mainly by anthropogenic activities. There are also natural factors that contribute to the increase such as higher water clarity levels and lower flushing rates. There are many indicators of the eutrophication process that include high levels of chlorophyll-a, nutrients (mainly total nitrogen (TN) and total phosphorus (TP), turbidity, and dissolved oxygen.

Chlorophyll-a is the green pigment that is found in all plants. Therefore, it's used as an indication of the presence of algae. High levels of chlorophyll-a are used as an indication of algal bloom. The availability of nutrients in fixed ratios is essential for algal growth.

Table 4: Summary of chlorophyll-a models developed in different studies for use with broad-band satellites imagery

No.	Satellite	Atm. correction	Model	Chl-a ($\mu\text{g/l}$)	R^2	Reference
1	LandSat TM	Image-based inversion developed by Gilabert (1994)	$\text{Chl-a} = 9.82 * ((\rho_b - \rho_r) / \rho_g)$	1.9-6.01	0.818	[40]
2	LandSat TM	None	$116.98 * (\text{IR} / \text{R}) - 29.709$	6-60	0.67	[38]
3	LandSat ETM+	COST	$\text{Log}_{10}(\text{chl-a}) = -10.476 \log_{10}((\rho_1 / \rho_3) + \rho_2 + \rho_3 + \rho_4 + \rho_5 + \rho_6) + 3.7331$	1-23	0.62	[41]
4	Terra ASTER	None	Multiple linear regression	0.3-4.2	0.86	[1]
5	IKONOS	ATCOR2	Multiple linear regression	<3	0.97	[42]
6	DubaiSat-1	Surface normal and surface roughness	Multiple linear regression	0.1-32.8	0.891	[4]

Excessive amounts of nutrients in the water are one main factor that accelerates algal growth to the extent that it can become blooms.

Total nitrogen is comprised of different organic and inorganic forms. Total phosphorus comes from many anthropogenic sources such as untreated or partially treated sewage and pharmaceutical waste. Total phosphorus is composed of particulate and dissolved phosphorus and is usually the limiting nutrient in most water bodies. Water clarity plays an important role in this process as turbid waters can harm certain forms of aquatic life. A depleted dissolved oxygen level that is caused by decomposition of organic materials is an indicator of the eutrophication process. Depletion of oxygen levels below certain point may cause death in aquatic life.

Relating a main eutrophication indicator in an area to other parameters that play a role in the eutrophication process is an empirical data-driven process. That is, if more data is available for the analysis, it will allow for better understanding of the relationships amongst the parameters. One of the large-scale studies carried out in the past few years utilized more than 500 data points to study the relationship between salinity and chlorophyll-a. The study concluded that salinity has an impact on both chl/TN and chl/TP values. An empirical relationship between chlorophyll-a and total phosphorus was developed in this study with an R-squared value of 0.73 using a linear equation [45]. In another study, 300 data points were used to model the relationship between chlorophyll-a and total phosphorus through non-linear regression and obtained an R-squared value of 0.67 [46].

3 Materials and Methodology

3.1 Materials

3.1.1 Satellite image

The WorldView-2 satellite image used in this study was acquired on the 24th of July, 2012 and it covered the study area: the Dubai Creek (Figure 3). The Dubai Creek extends from the Dubai coast upstream and forms a lagoon downstream. The Creek passes under Al-Gharhoud Bridge and The Floating Bridge and embraces Port Saeed, Ras Al Khor Wildlife Sanctuary, and some malls and hotels. WorldView-2 images are 11-bit images scaled to 8-bit or 16-bit in eight multispectral bands and one panchromatic band. The pixel size is 2x2 meters in the multispectral bands and 0.5x0.5 meters in the panchromatic band.

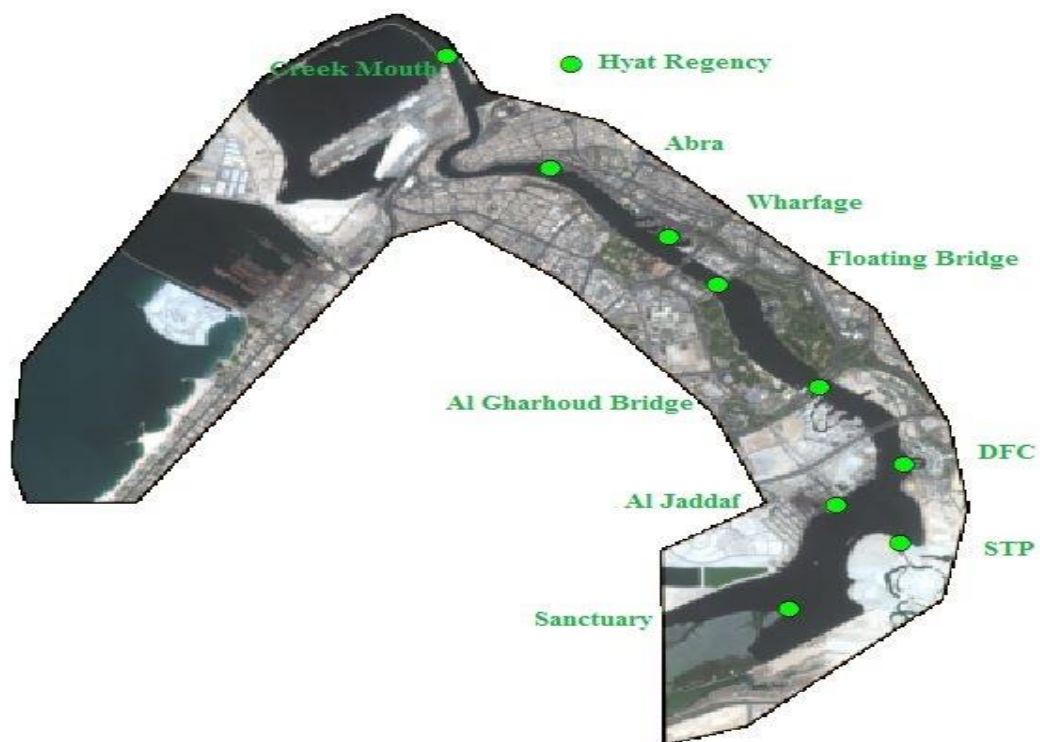


Figure 3: The extents of the WorldView-2 imagery showing the Dubai Creek and the water quality monitoring stations

3.1.2 In-situ data

There are 10 monitoring stations located along Dubai Creek that are used by the Dubai Municipality (DM) to record water quality parameters. The DM water quality

data used in this study was provided as quarters averages (every three months) (Tables 5 and 6). The water quality parameters measured by these stations include chlorophyll-a, total nitrogen, nitrates, phosphates, dissolved oxygen (concentration and %), turbidity, pH, and salinity. Figure 3 illustrates the locations of the measurement stations on the WorldView-2 image.

3.2 Methodology

The WorldView-2 image was first reprojected to the Dubai Local Transverse Mercator (DLTM), the DNs were converted to radiance values, and the COST atmospheric correction algorithm was then applied. Then, a band-ratio model to estimate chlorophyll-a concentrations was developed and validated with the interpolated in-situ data. Also, another model was developed to correlate chlorophyll-a and eutrophication indicators.

3.2.1 Image pre-processing

Before WorldView-2 images were processed to derive chlorophyll-a values in the study area, they were first preprocessed by correcting for geometric, radiometric, and atmospheric errors. Also, chlorophyll-a field data were interpolated based on the assumption that the data of each quarter is a good indication of the midpoint values of the quarter. The following subsections describe the pre-processing procedures implemented on the WorldView-2 images.

3.2.1.1 Geometric Correction

The objective of geometric correction was to ensure that locations of points in the satellite image matched their locations on ground. The acquired WorldView-2 image was delivered in the UTM (Universal Transverse Mercator) zone 40 North with WGS84 as a Datum. A decision was made to re-project the images into the DLTM (Dubai Local Transverse Mercator), which is the coordinate system of the in-situ data. The ESRI's ArcMap 9.3 was used to re-project the satellite image into the DLTM. The parameters needed to re-project the image to DLTM are shown in Table 7 [4].

Table 5: Water quality data - Quarter 2, 2012

Station name	Northing N	Easting E	Salinity ppt	pH	Chlorophyll mg/L	DO+%	DO+ Conc mg/L	Turbidity N.T.U	nitrates as N mg/L	Total Nitrogen mg/L	Phosphates as P mg/L
Creek mouth	2797486.926	495784.713	39.72	7.9	4.6	85.9	5.08	1	<0.05	0.52	0.01
Hyat Regency	2797345.594	497360.633	39.08	8	15.3	109.2	6.66	1	<0.05	0.69	0.02
Abra	2795589.528	497081.315	38.43	8	5.9	59.8	3.65	1	0.26	1.61	0.1
Wharfage	2794425.83	498580.139	38.41	8	4.6	60.6	3.71	1	0.31	1.74	0.1
Floating Bridge	2793618.334	499199.91	34.84	8.5	57.5	169.7	10.91	2	1.76	2.9	0.26
Al Garhoud Bridge	2791886.821	500486.441	36.55	8.3	57.8	159.8	10.27	2.5	2.34	3.72	0.39
Dubai Festival City	2790567.425	501537.84	34.7	8.6	69.5	236.3	15.06	2.5	1.52	2.43	0.21
STP Outfall	2789243.037	501506.922	35.33	8.6	69.3	160.3	10.25	2.5	1.13	2.03	0.18
Al Jaddaf	2789892.243	500705.415	35.29	8.6	74.8	218.1	13.93	3	1.05	2.08	0.18
Sanctuary	2788144.426	500113.385	36.02	8.7	92.6	243.8	15.41	3	0.42	1.05	0.08

Table 6: Water quality data - Quarter 3, 2012

Station Name	Northing N	Easting E	Salinity ppt	pH	Chlorophyll mg/L	DO+% mg/L	DO+ Conc mg/L	Turbidity N.T.U	nitrates as N mg/L	Total Nitrogen mg/L	Phosphates as P mg/L
Creek mouth	2797486.926	495784.713	40.42	7.7	1.3	82.2	4.68				
Hyat Regency	2797345.594	497360.633	40.48	7.7	6	71.5	4.1	1	0.07	0.58	0.02
Abra	2795589.528	497081.315	40.01	7.8	42	71.8	4.1	1.5	0.16	0.7	0.04
Wharfage	2794425.83	498580.139	39.75	7.8	4.8	59.3	3.4	1.5	0.17	0.78	0.04
Floating Bridge	2793618.334	499199.91	39.43	8	18.8	83.5	4.74	1.5	0.17	0.65	0.05
Al Garhoud Bridge	2791886.821	500486.441	38.73	8.1	33.9	116.4	6.6	2	0.13	0.63	0.04
Dubai Festival City	2790567.425	501537.84	38.42	8.1	34.5	83.4	4.74	2.5	0.17	0.64	0.05
STP Outfall	2789243.037	501506.922	38.41	8.2	36.8	120	6.79	2	0.3	1.42	0.03
Al Jaddaf	2789892.243	500705.415	37.47	8.3	37.9	132.1	7.55	2	0.36	1.35	0.08
Sanctuary	2788144.426	500113.385	37.99	8.2	18.8	86	4.9	2	0.06	0.99	0.08

3.2.1.2 Radiometric Correction

WorldView-2 images were delivered free of radiometric errors. Therefore, the DNs (Digital Numbers) were converted to TOA (Top-Of-Atmosphere) spectral radiance without the need for radiometric corrections. The equation utilized for this purpose was provided by Digital Globe and is shown below [43]:

$$L_{\lambda_{\text{pixel,band}}} = \frac{K_{\text{band}} \times q_{\text{pixel,band}}}{\Delta\lambda_{\text{band}}} \quad (1)$$

Table 7: DLTM projection parameters [4]

Name	DLTM (Dubai Local Transverse Mercator)
False Easting	500000
False Northing	0
Central meridian	55.334
Scale factor	1
Latitude of Origin	0
Linear Unit	Meter

where:

$L_{\lambda_{\text{pixel,band}}}$: is the top-of-atmosphere spectral radiance for a band.

K_{band} : is the absolute radiometric calibration factor.

$q_{\text{pixel,band}}$: is the radiometrically corrected image pixels.

$\Delta\lambda_{\text{band}}$: is the effective bandwidth for a band.

The absolute radiometric calibration factors and the effective bandwidths for each band are provided in the metadata file included with the satellite image (Table 8).

ERDAS Imagine 2011's Model Maker was used to calculate TOA spectral radiance for each pixel of the 8-band WorldView-2 image (Figure 4). The ERDAS Imagine Model Maker consists of three parts; the input, the process, and the output. The input defines the image upon which mathematical calculations will be conducted.

Table 8: Absolute radiometric calibration factor and effective bandwidth for each of WorldView-2 band

Band	Absolute radiometric calibration factor(K_{band})	Effective bandwidth ($\Delta\lambda_{\text{band}}$)
Coastal	$9.295654e^{-3}$	$4.730000e^{-2}$
Blue	$1.783568e^{-2}$	$5.430000e^{-2}$
Green	$1.364197e^{-2}$	$6.300000e^{-2}$
Yellow	$6.810718e^{-3}$	$3.740000e^{-2}$
Red	$1.851735e^{-2}$	$5.740000e^{-2}$
Red-edge	$6.063145e^{-3}$	$3.930000e^{-2}$
NIR1	$2.050828e^{-2}$	$9.890000e^{-2}$
NIR2	$9.042234e^{-3}$	$9.960000e^{-2}$

The output defines the image after performing the calculations. Finally, the process defines the functions, constants, and tabular values that are needed to process the input into the desired output.

3.2.1.3 Atmospheric Correction

Atmospheric correction was the last step in the pre-processing of satellite images. It was decided to use the COST method to perform atmospheric correction due to its simplicity and the successful results it produces. The mathematical expression of the COST method is as follows [23]:

$$\rho_{\lambda_{\text{pixel,band}}} = \frac{(L_{\lambda_{\text{pixel,band}}} - L_{\lambda_{\text{haze,band}}}) \times d_{\text{ES}}^2 \times \pi}{E_{\text{sun}\lambda_{\text{band}}} \times \cos(\theta_s)} + 0.01 \quad (2)$$

where:

$\rho_{\lambda_{\text{pixel,band}}}$: is atmospherically-corrected reflectance.

$L_{\lambda_{\text{pixel,band}}}$: top-of-atmosphere spectral radiance.

d_{ES} : Earth-sun distance.

$E_{sun, \text{band}}$: band-averaged solar spectral irradiance (provided by DigitalGlobe®) (Table 9).

θ_s : solar zenith angle (Radian)

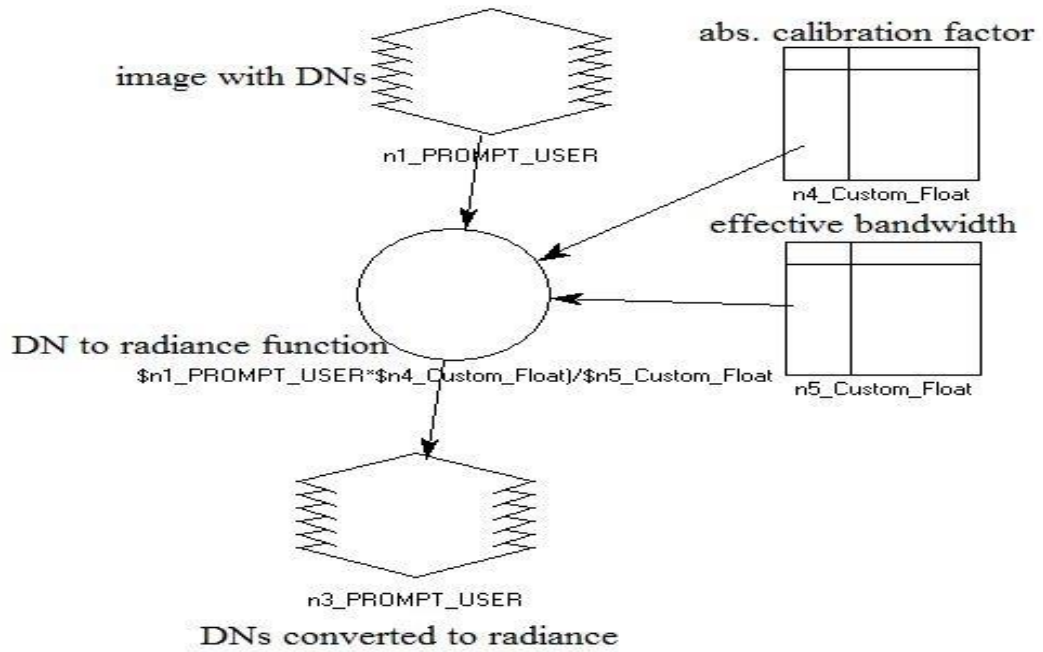


Figure 4: Model created in ERDAS Imagine to convert DNs to Radiance

Table 9: Band-averaged solar spectral irradiance values for WorldView-2 bands

Spectral band	Spectral irradiance ($W \cdot m^{-2} \cdot (\text{micro})m^{-1}$)
Panchromatic	1580.8140
Coastal	1758.2229
Blue	1974.2416
Green	1856.4104
Yellow	1738.4791
Red	1559.4445
Red-edge	1342.0695
NIR1	1069.7302
NIR2	861.2866

The earth-sun distance calculation is performed as [43]:

$$d_{ES} = 1.00014 - 0.01671 \times \cos(g) - 0.00014 \times \cos(2g) \quad (3)$$

where $0.983 < d_{ES} < 1.017$ AU.

$$g = 357.529 + 0.98560028 \times D \quad (4)$$

$$D = JD - 2451545 \quad (5)$$

where JD is the Julian day of the scene.

$$JD = \text{int}(365.25 \times (\text{year} + 4716)) + \text{int}(30.6001 \times (\text{month} + 1)) + \text{day} + \frac{UT}{24} + B - 1524.5 \quad (6)$$

where int is an integer number (Ignore decimals)

Year, month, and day represent the acquisition time of the scene.

$$B = 2 - A + \text{int} \frac{A}{4} \quad (7)$$

$$A = \text{int} \frac{\text{year}}{100} \quad (8)$$

$$UT = hh + \frac{mm}{60} + \frac{ss.ddddd}{3600} \quad (9)$$

where h,m, s, and d are the hour, minute, second, and second decimals of the scene acquisition time. UT is the universal time of the scene.

$$\theta_s = 90.0 - \text{sunEL} \quad (10)$$

where sunEL is the sun elevation at the time of acquisition of the scene.

The interpolation of field chlorophyll-a values was done as following:

$$\text{Int. Chl} - a = \frac{\text{chl-a}_{\text{quarter 2}} - \text{chl-a}_{\text{quarter 3}}}{4} \quad (11)$$

Determination of $L_{\lambda_{\text{haze,band}}}$ is to be based on the minimum non-zero radiance value from each band that has 100 or more pixels. Information about pixel values can be extracted from the images using the Raster Attribute Editor in ERDAS Imagine.

Figure 5 shows the model built in ERDAS Imagine to perform the atmospheric correction.

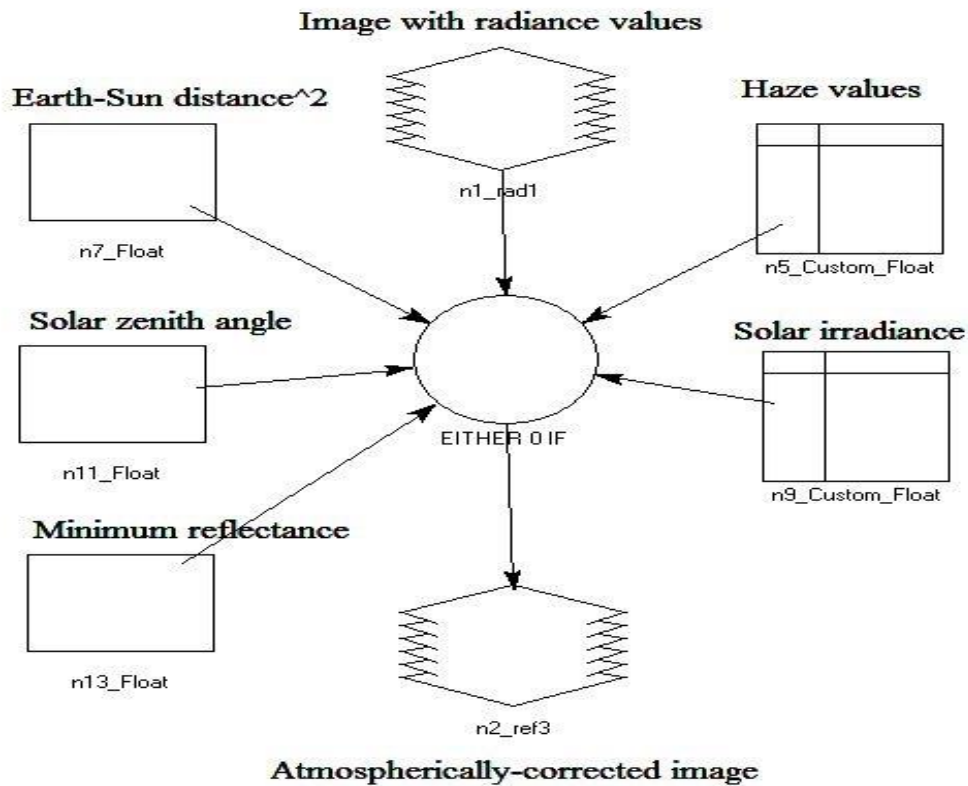


Figure 5: COST model developed for ERDAS Imagine to perform the atmospheric correction

3.2.2 Chlorophyll-a Spectral Modelling

In order to develop the chlorophyll-a spectral model, different simple band ratios of ground-leaving reflectance values of the eight WorldView-2 bands were used. These ratios were tested against the field values of chlorophyll-a. The different band ratio combinations included two-band, three-band, and four-band ratios. The strength of the correlation between the model and the field results were based on R-squared values. The model that performed the best was applied to the entire scene using the Model Maker in ERDAS Imagine 2011 as shown in Figure 6. The produced map was then colour coded using ArcGIS 9.3.

3.2.3 Modelling the Relation between Field Chlorophyll-a and Eutrophication Indicators

A regression model was developed by using a spreadsheet that related chlorophyll-a to various eutrophication parameters. These parameters included total nitrogen, phosphates (due to the absence of total phosphorus in-situ data), dissolved oxygen, and salinity. The models tested included either one of the parameters versus chlorophyll-a or a ratio of two of the parameters versus values of chlorophyll-a. Eutrophication indicators in quarter 2, 2012 were empirically tested against interpolated chlorophyll-a data. These tested indicators included salinity, dissolved oxygen, total nitrogen, phosphates, and a ratio of any two of them. The model with the highest R-squared value was selected for relating it with the chlorophyll-a spectral model.

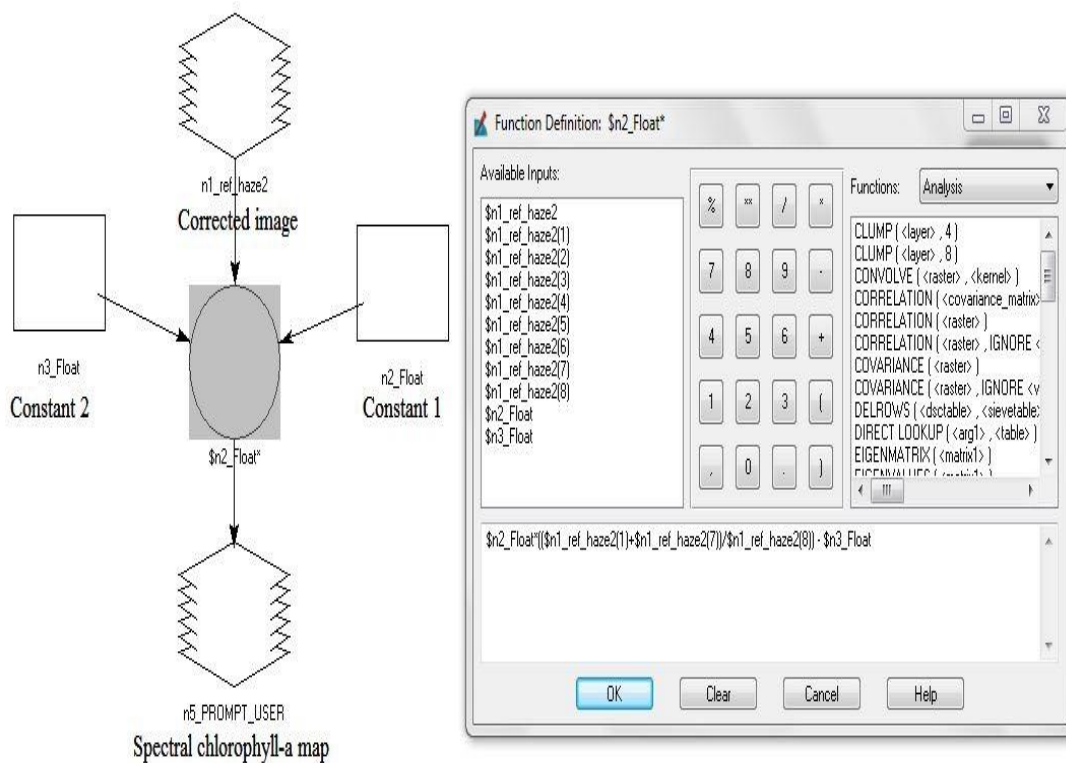


Figure 6: Spectral chlorophyll-a map generation using ERDAS Imagine 2011

3.2.4 Modelling Spectral Characteristics of Water Columns to Their Content of Eutrophication Indicators

The model developed to estimate chlorophyll-a from spectral characteristics of water columns was combined with the best-fit model that relates field chlorophyll-a to one or more of the eutrophication indicators. Chlorophyll-a values that were produced as a map earlier were used as an input for this model using the ERDAS Imagine 2011 model maker along with the model developed in the previous section to produce a map of the best-fit eutrophication parameters as seen in Figure 7. Figure 8 summarizes the process followed in this study.

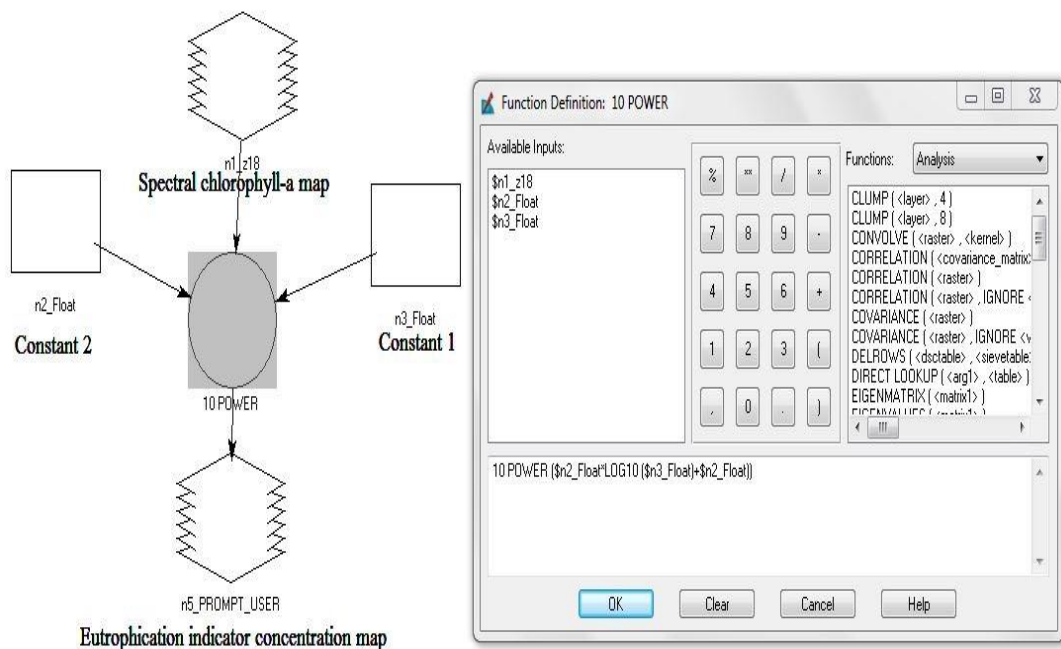


Figure 7: Eutrophication indicators map generation using ERDAS Imagine 2011

3.3 Study Limitations

This study was conducted with few limitations. One of the limitations is the small number of monitoring stations available for the modelling process. The other limitation is the unavailability of daily averaged field data, rather, quarterly averaged data were provided.

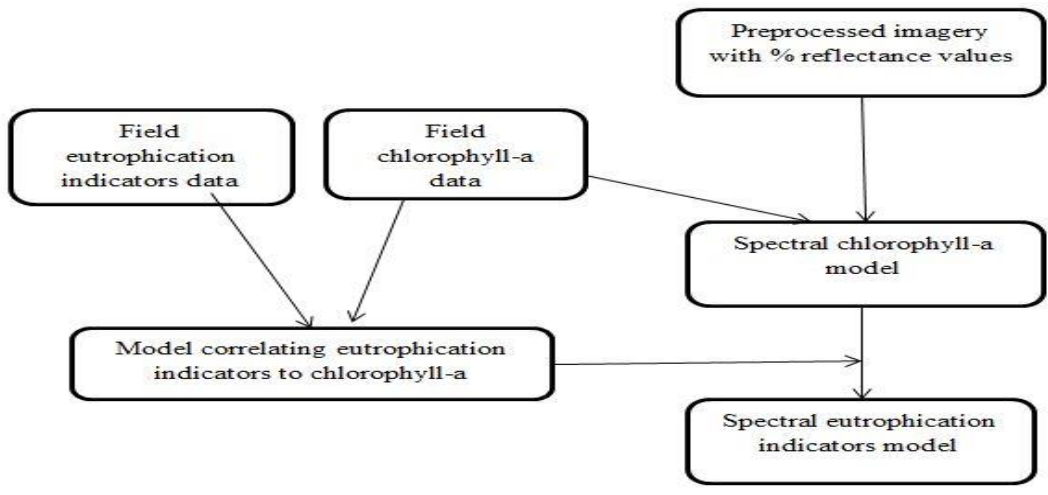


Figure 8: A flow chart summarizing the steps used in this study

4 Results and Discussion

4.1 Data Preparation and Image Preprocessing

Chlorophyll-a data were provided by the Dubai Municipality as quarterly values. Therefore, obtaining chlorophyll-a concentrations at the day of the satellite image acquisition wasn't possible. An interpolation of the provided quarterly data was performed so that chlorophyll-a concentrations at the day of the image acquisition could be approximately estimated. Equation 11 was used for the interpolation of the data and the results are shown in Table 10.

Table 10: Quarterly and interpolated chlorophyll-a values

Station	Chl-a Quarter 2, 2012 $\mu\text{g/l}$	Chl-a Quarter 3, 2012 $\mu\text{g/l}$	Interpolated Chl-a value $\mu\text{g/l}$
Creek Mouth	4.6	1.3	2.13
Hyatt Regency	15.3	6	8.33
Abra	5.9	42	32.98
Wharfage	4.6	4.8	4.75
Floating Bridge	57.5	18.8	28.48
Al Gharhoud Bridge	57.8	33.9	39.88
Dubai Festival City	69.5	34.5	43.25
STP Outfall	69.3	36.8	44.93
Jaddaf	74.8	37.9	47.13
Sanctuary	92.6	18.8	37.25

Two of the ten monitoring stations located on the creek were excluded from the study. These two stations were the Hyatt Regency and Al-Gharhoud Bridge monitoring stations. The Hyatt Regency station was excluded because it was located outside the WorldView-2 satellite image. The Al-Gharhoud Bridge station was excluded because the monitoring station was located under the bridge which means that the pixel representing the location of the station spectrally represents the concrete barrier of the bridge rather than the water column below the bridge. All the modelling

and analysis efforts performed in this study were based on the data of the remaining eight stations.

Atmospheric correction was performed in order to convert the top-of-atmosphere radiance values to ground-leaving reflectance values. Equations 3 through 10 combined with spectral irradiance values in Table 9 were used to calculate the various input values needed to apply equation 2 and generate an atmospherically corrected satellite image. The selection of haze values in the equation was based on the first DN value with 100 or more pixels. These values are shown in Table 11 and were extracted from the image histogram in ERDAS Imagine 2011 (Figure 9). Selection of the haze value as the lowest non-zero value is not an accurate representation of haze values; rather it only represents noise in the imagery and, therefore, the selection should be based on higher values with higher frequencies [47].

Table 11: DN and radiance values of haze selected for the COST atmospheric correction method

Band	DN of haze	Radiance of haze
Coastal Blue	416	81.74
Blue	239	78.50
Green	267	57.82
Yellow	219	39.88
Red	92	29.68
Red-Edge	126	19.44
Near Infrared 1	58	12.03
Near Infrared 2	81	7.35

Row	Value	Histogram	Opacity
393	394	16	1
394	395	15	1
395	396	17	1
396	397	14	1
397	398	25	1
398	399	21	1
399	400	27	1
400	401	26	1
401	402	27	1
402	403	34	1
403	404	26	1
404	405	39	1
405	406	45	1
406	407	43	1
407	408	56	1
408	409	40	1
409	410	57	1
410	411	55	1
411	412	73	1
412	413	78	1
413	414	95	1
414	415	84	1
415	416	121	1
416	417	132	1
417	418	170	1
418	419	181	1

Figure 9: Band 1 (coastal blue) DN of haze selection

4.2 Spectral Chlorophyll-a Modelling

After preprocessing the satellite image and conversion of the pixel values from DNs to ground-leaving reflectance, various models were developed to map chlorophyll-a concentrations in Dubai Creek at the time when the image was acquired. The models consisted of simple band ratios of ground-leaving reflectance values of the eight WorldView-2 bands. These models included two-band, three-band, and four-band models; however, three-band models performed the best (based on the obtained R-squared values) among the developed models. Descriptions of the main features of each WorldView-2 eight band in relation to vegetation mapping generally, and to chlorophyll-a specifically are given in Table 12.

Regression analysis was used to evaluate every model against the in-situ data shown in Table 10. Out of the many models developed using simple band rationing, only a few showed good to very good R-squared values. The five best performing models based on the highest squared values obtained are shown in Figure 10 to 14.

Table 12: WorldView-2 bands description [33]

Band	Description
Coastal Blue	Absorbed by chlorophyll in healthy plants and aids in conducting vegetative analysis
Near Infrared 1	Effectively separates water bodies from vegetation
Near Infrared 2	Enables broader vegetation analysis and biomass studies
Blue	Readily absorbed by chlorophyll in plants
Green	Focus on peak of reflectance in healthy vegetation
Yellow	Detects yellowness of vegetation both in land and in water
Red edge	centered at the high reflectivity portion of vegetation response
Red	Focused on the absorption of red light by chlorophyll in healthy plant

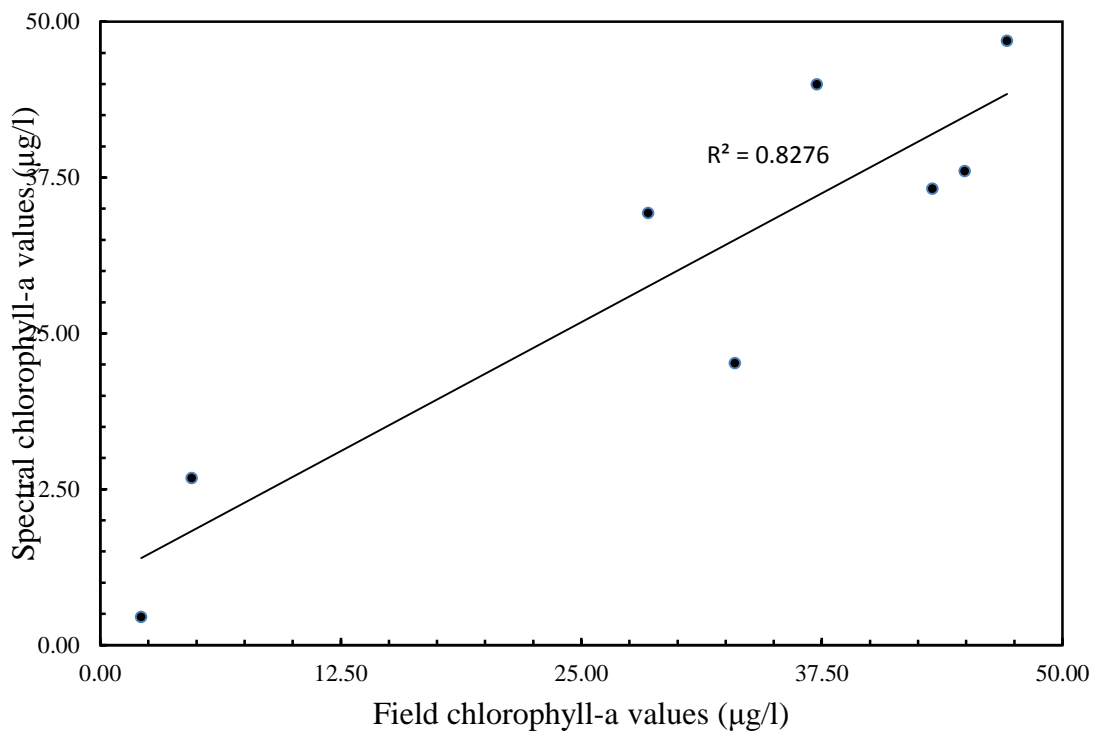


Figure 10: Correlation between field and spectral chlorophyll-a values
(CB+NIR1)/NIR2

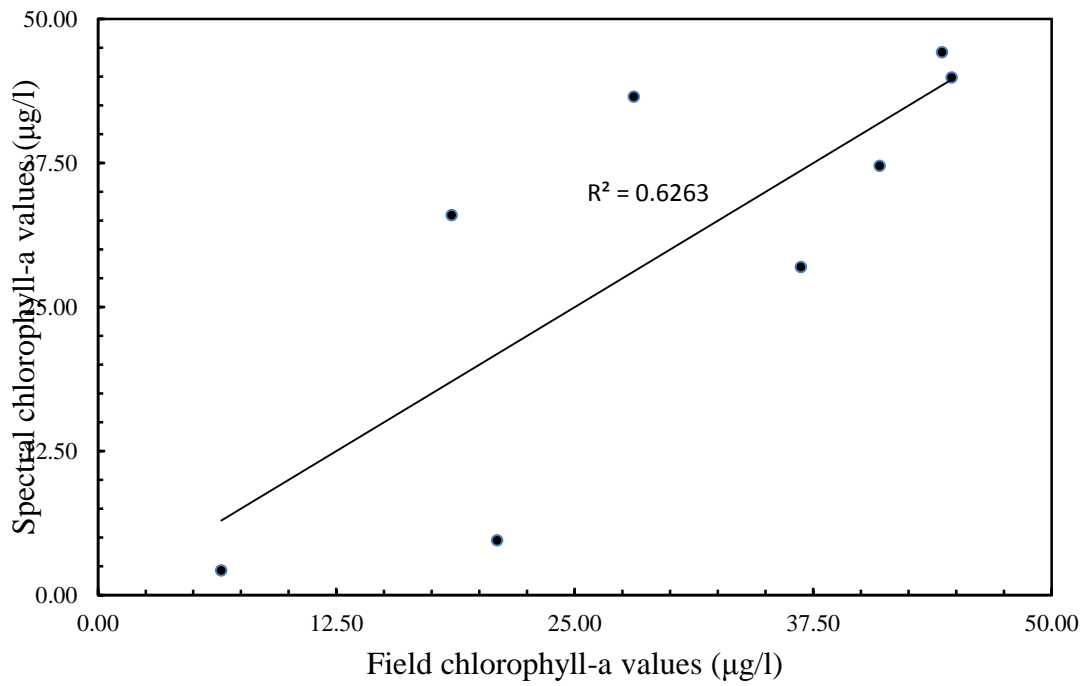


Figure 11: Correlation between field and spectral chlorophyll-a values
(B+NIR1)/NIR2

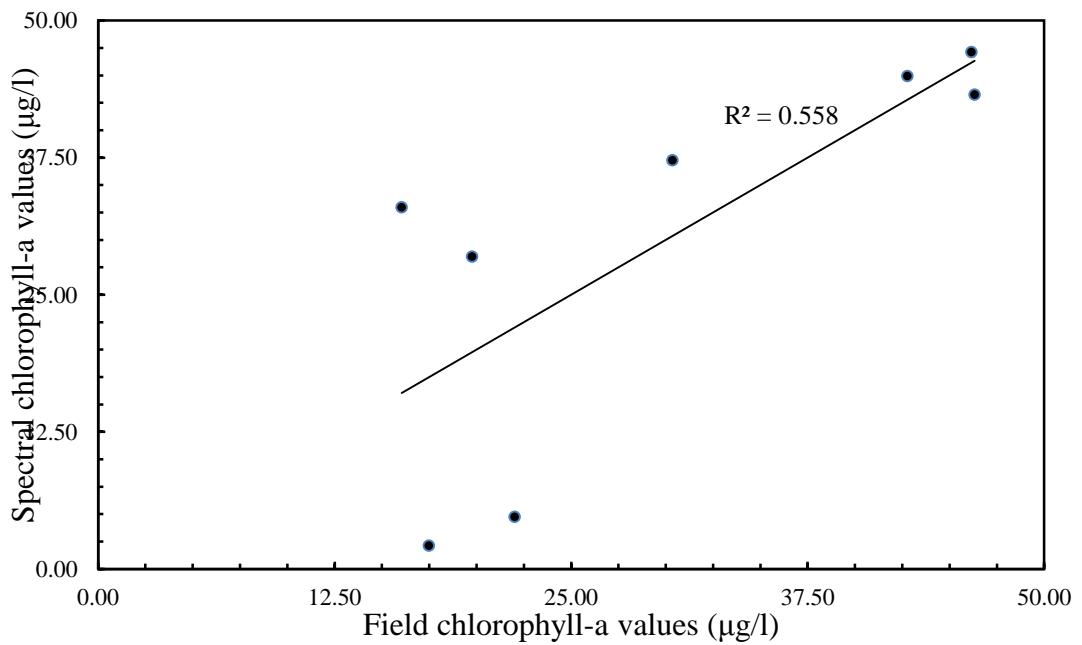


Figure 12: Correlation between field and spectral chlorophyll-a values
(G+NIR1)/NIR2

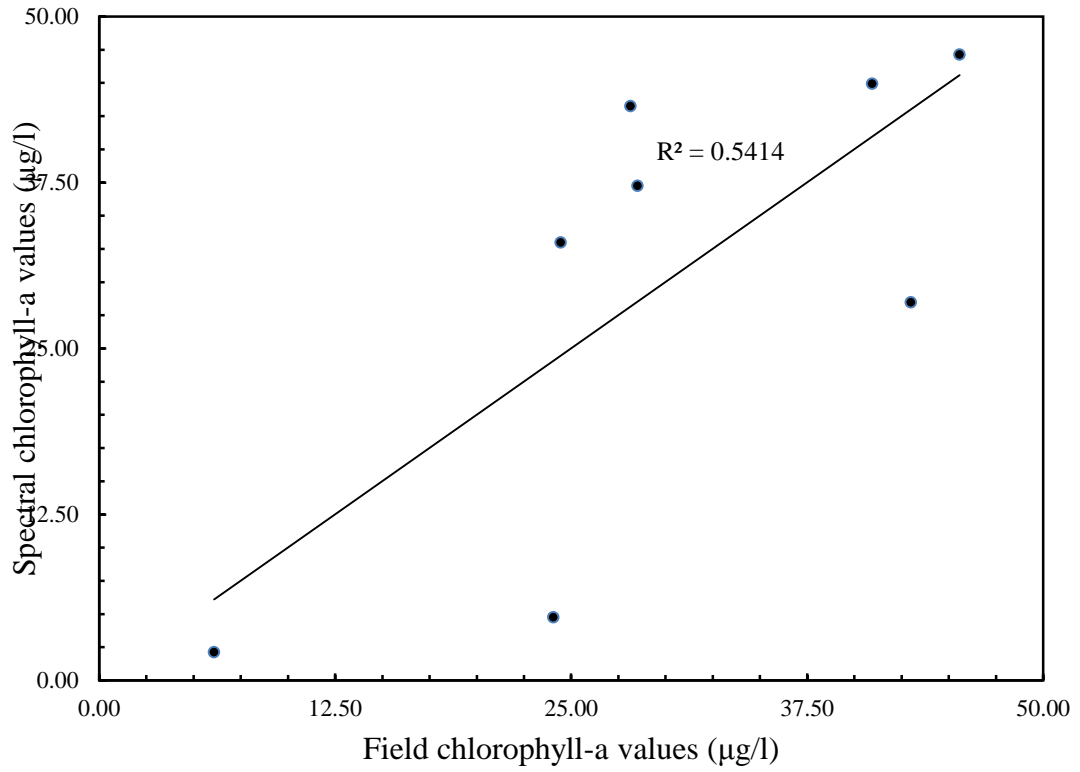


Figure 13: Correlation between field and spectral chlorophyll-a values
(Y+NIR1)/NIR2

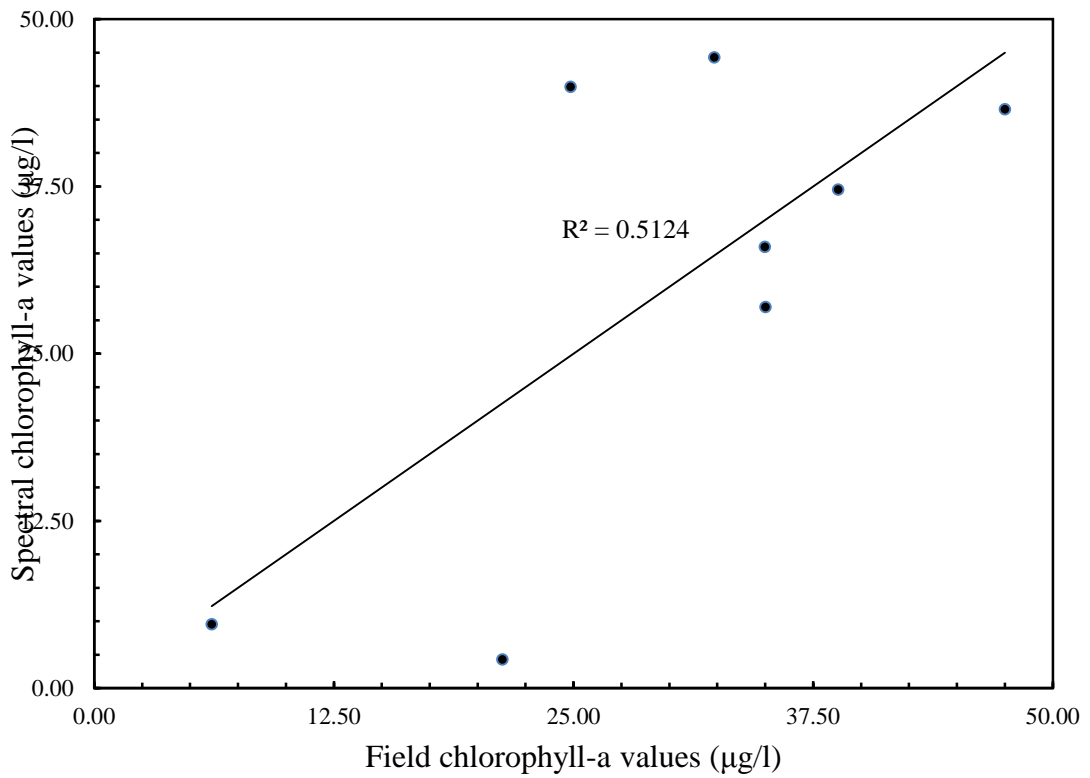


Figure 14: Correlation between field and spectral chlorophyll-a values (B+NIR1)/RE

It's important to note that these models mostly include a combination of NIR1 and NIR2 (Near Infrared 1 and 2, respectively) bands. Evidently, NIR1 is effective in separating water from vegetation and NIR2 enables for broader vegetation analysis and biomass studies which explains the importance of these two bands in chlorophyll-a mapping and justifies their appearance in most of the models. The best performing model included the Coastal Blue band which is absorbed by chlorophyll and aids in conducting vegetative analysis as stated in Table 12. Table 13 lists the top models ordered based on the R-squared values obtained in each case. Note that the band name in the table refers to the ground-leaving reflectance value of that band.

The best model is listed below:

$$\text{Spectral chlorophyll} - a = 243.06 \times \frac{\text{CB} + \text{NIR1}}{\text{NIR2}} - 429.6 \quad (12)$$

where: CB, NIR1, and NIR2 are ground-leaving reflectance values of the coastal blue, near infrared 1, and near infrared 2 of the WorldView-2 spectral bands.

Table 13: Best performing models along with their R-squared values

Band Ratio	R-squared (%)
(Coastal blue + Near infrared 1)/Near infrared 2	82.7
(Blue + Near infrared 1)/Near infrared 2	62.6
(Green + Near infrared 1)/Near infrared 2	55.8
(Yellow + Near infrared 1)/Near infrared 2	54.1
(Red edge + Near infrared 2)/Near infrared 1	52.9
(Blue + Near infrared 1)/Red edge	51.2
(Yellow + Red)/Red edge	45.9
Near infrared 1/Near infrared 2	43.3
Red edge/Near infrared 1	41.3
Yellow/Red edge	31.9

Comparing the model developed in this study with the models developed in other similar studies mentioned in Table 4, the R-Squared value in this study is better than

some of them. Also, the range of chlorophyll-a data that were used to develop the model is higher than all of the referenced studies.

A comparison of the spectral-based and in-situ chlorophyll-a concentrations at the eight monitoring stations is shown in Table 14. The percent errors between the two values were computed and are shown in column 4 of Table 14. These percentages between the field and the spectral chlorophyll-a concentrations vary among the stations as shown in the table.

Table 14: Field and spectral differences of chlorophyll-a values

Station	Field chlorophyll-a $\mu\text{g/l}$	Spectral chlorophyll-a $\mu\text{g/l}$	% Error
Creek Mouth	2.13	2.24	5.16
Abra	32.98	22.61	31.44
Wharfage	4.75	13.4	182.10
Floating Bridge	28.48	34.65	21.66
Dubai Festival City	43.25	36.6	15.38
STP Outfall	44.93	38.01	15.4
Jaddaf	47.13	48.48	2.86
Sanctuary	37.25	44.98	20.75

The lowest differences were obtained at the Creek Mouth and Jaddaf stations as 0.11 and 1.35, respectively. The highest difference was 10.37, which was obtained at the Abra station. These differences are large at some of the stations. However, it's important to note that this study attempted modeling for a bigger range of chlorophyll-a values compared to other studies such as the study conducted by Brivio [40].

The model in Equation 12 was applied to the entire creek using ERDAS Imagine 2011's model maker to generate a spectral chlorophyll-a concentration map. The map was color-coded in ArcMap and is shown in Figure 15. As depicted in this figure, most of the creek has chlorophyll-a concentrations in the range of 20-40 $\mu\text{g/l}$. Low concentrations of less than 20 $\mu\text{g/l}$ are observed in the middle of the creek, which

could be because there are no anthropogenic activities along this segment of the creek. The “lagoon” section of the creek has the highest concentrations in the range of 30-50 µg/l. There are two factors that contribute to these high concentrations in this part of the creek, which are (a) the poor circulation and flushing and (b) the location of the effluent discharging point of the Al Awir wastewater treatment plant. The concentrations of chlorophyll-a found along the creek are alarming. According to the Organization for Economic Cooperation and Development (OECD), the mean threshold value for chlorophyll-a should not exceed 8 µg/l [48]. It is well noted that chlorophyll-a concentrations in the creek are above this number in most parts, and for this reason corrective measures are needed. Another concerning fact about chlorophyll-a levels in the creek are related to year-after-year changes in chlorophyll-a concentrations and are presented in Table 15.

It is also important to note the changes in chlorophyll-a concentrations in Dubai Creek over the last few years. For example, in quarter 2 data of 2010, 2011, and 2012 presented in Table 15, the recorded concentrations at five monitoring stations are at alarming levels. Given this data, the highest annual value of chlorophyll-a seems to be increasing year after year. If this trend continues at the same rate, the creek will suffer major negative consequences. The averages of the concentrations increased from 2010 where it was about 6.84 µg/l which is below the OECD threshold of 8 µg/l. However, in both 2011 and 2012 the average concentrations exceeded this threshold by 12.86 and 9.64 µg/l, respectively.

Table 15: Annual change in measured chlorophyll-a concentrations

Station	Chl-a Q2, 2010 (µg/l)	Chl-a Q2, 2011 (µg/l)	Chl-a Q2, 2012 (µg/l)
Creek Mouth	0.1	8.1	4.6
Hyatt Regency	10.8	11.2	15.6
Abra	6.4	29.8	5.9
Wharfage	9.2	32.8	4.6
Floating Bridge	7.7	22.4	57.5
Average	6.84	20.86	17.64

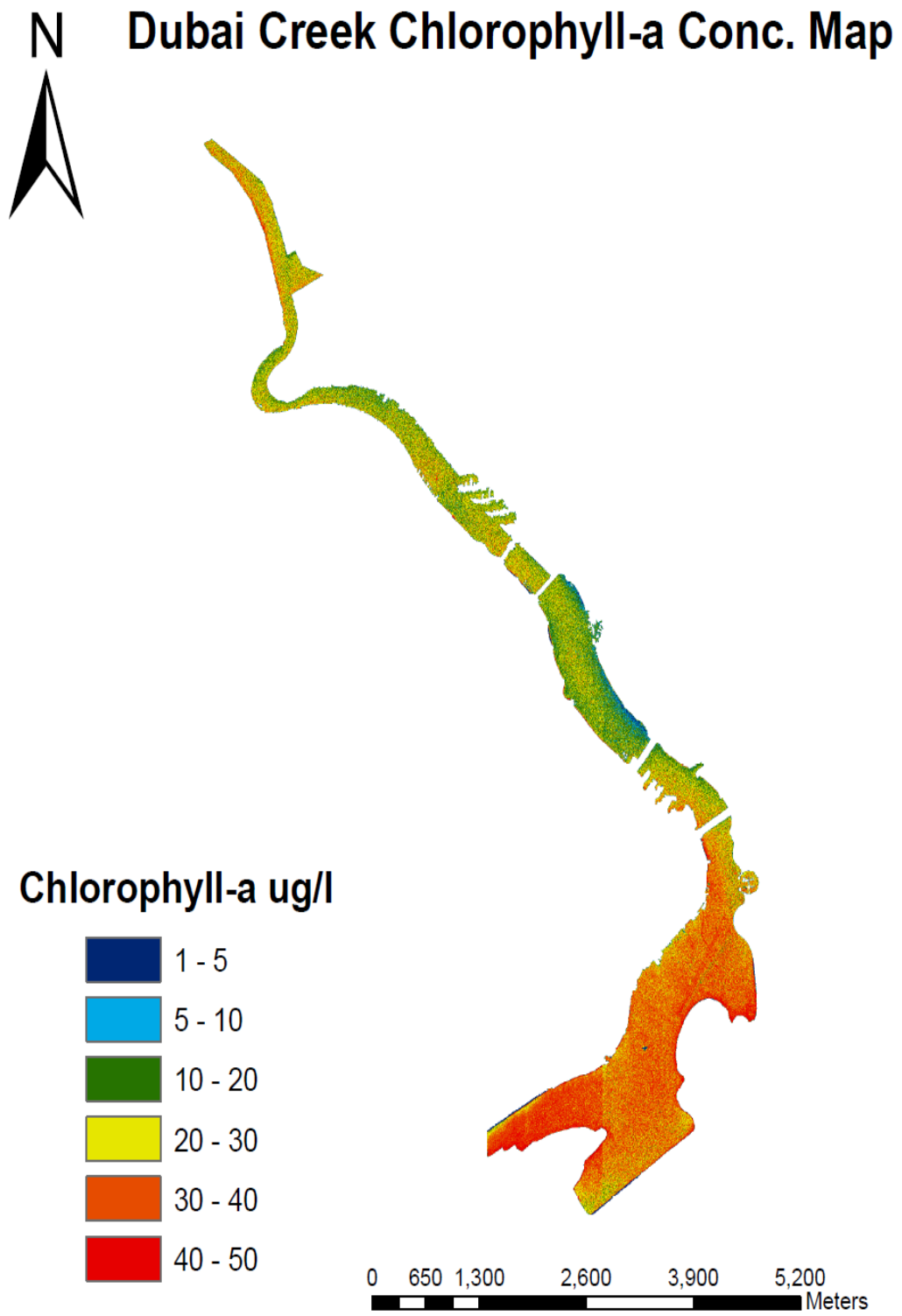


Figure 15: Spectral chlorophyll-a map

An increase of about 200% in 2011 was noticed followed by a slight decrease of about 15% in 2012.

Monitoring of chlorophyll-a concentrations in the creek and making sure they follow the designated thresholds is made easier by using remote sensing imagery and can be carried out very efficiently, covering the whole creek instead of only some points.

4.3 Empirical Relation between Chlorophyll-a and Eutrophication Indicators

The relationships between the field values of the eutrophication indicators in the creek and chlorophyll-a were analyzed. These indicators included total nitrogen, phosphates (due to absence of total phosphorus data), dissolved oxygen, and salinity. The analysis of relationships was carried out using simple regression models.

The eutrophication indicator data used was Q2, 2012 in-situ data. The cause-and-effect relationship between high levels of eutrophication indicators and high concentrations of chlorophyll-a is not immediate. This is due to the fact that an increase in algal growth is not necessarily immediate following a nutrient increase in an area. This model was developed in order to integrate it with the spectral chlorophyll-a model and produce concentration maps based on spectral characteristics of water columns.

The five regression models with the highest R-squared values are shown in Figures 16-20. The model that performed the best against field chlorophyll-a values from all the tested models is $\log(\text{total nitrogen/phosphates})$, which is shown in Figure 16, depicting a relationship of an inverse proportionality. This relationship indicates that an increase in the levels of total nitrogen without an increase in phosphates or a reduction in phosphates without a decrease in total nitrogen will not necessarily result in an increase in chlorophyll-a. Analysis results suggest that an excess of either total nitrogen or phosphates will not necessarily increase algal growth, which depends on both parameters. It's important to note that most of the total phosphorus found in water bodies comes from anthropogenic sources as opposed to total nitrogen which can come from other sources. Figure 17 shows the relationship between salinity and chlorophyll-a in the creek, which demonstrates the strong effect of salinity on algal

growth and further on the eutrophication process. Figure 18 depicts the relationship between salinity, phosphates and chlorophyll-a, which looks similar to the relationship obtained by Hakanson et al. [45]. Figure 19 shows the relationship between phosphates and chlorophyll-a, which suggests that total phosphorus is the limiting nutrient in this case, which explains the weak correlation between total nitrogen and chlorophyll-a in the creek. Figure 20 shows the relationship between total nitrogen, salinity, and chlorophyll-a, which show weak correlation similar to the outcome obtained by Hakanson et al. [45].

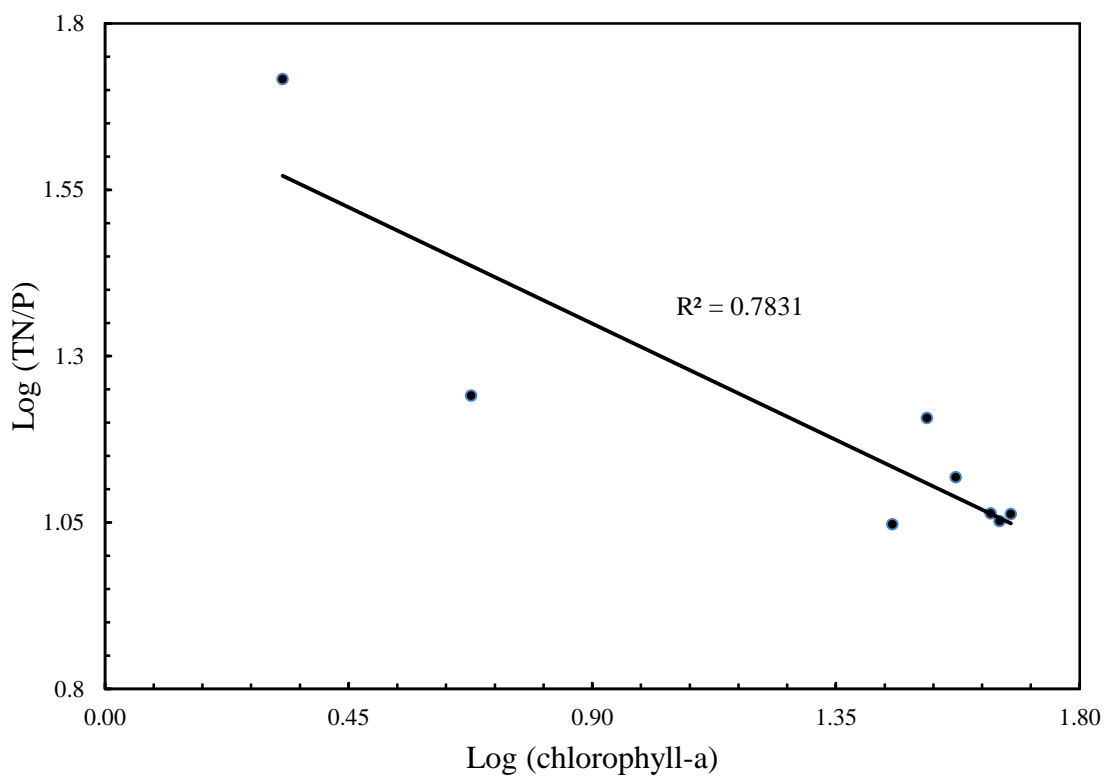


Figure 16: Correlation between eutrophication indicators and field chlorophyll-a (TN/P)

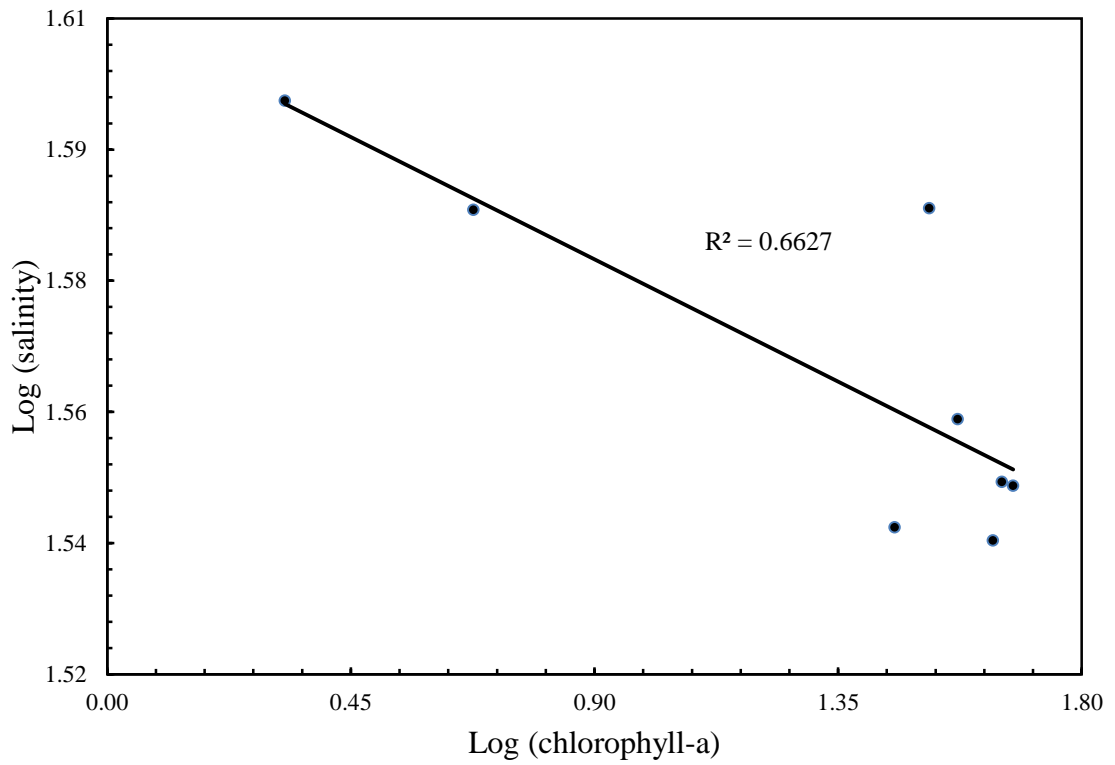


Figure 17: Correlation between eutrophication indicators and field chlorophyll-a (salinity)

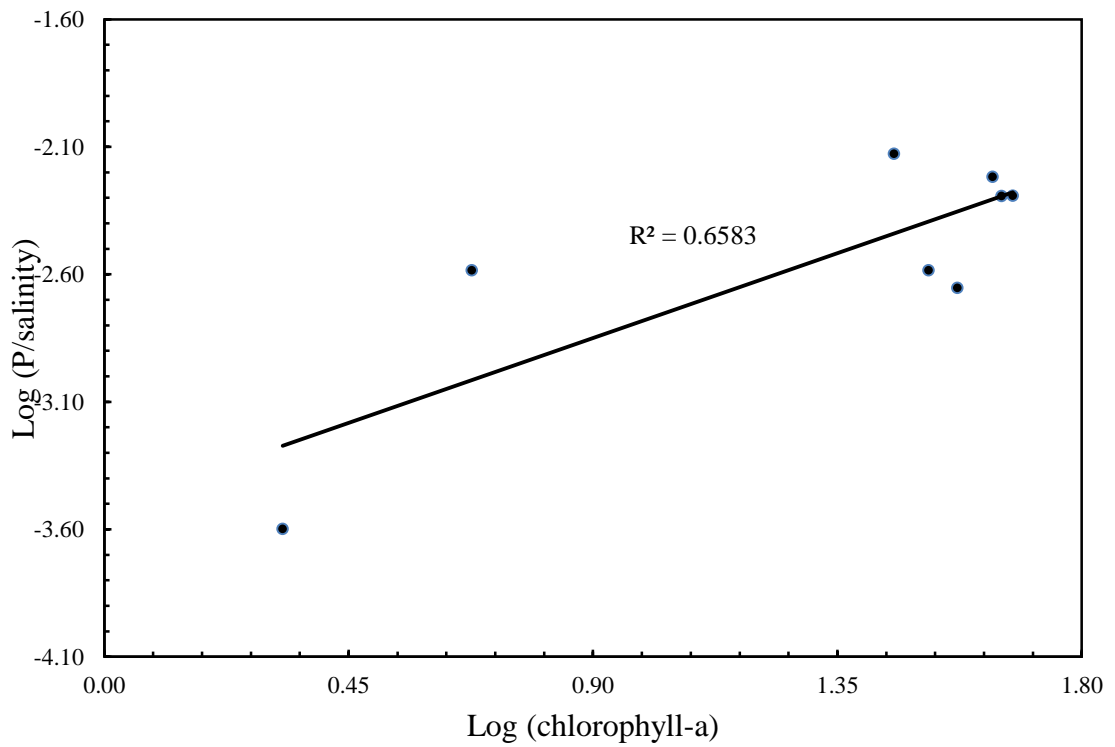


Figure 18: Correlation between eutrophication indicators and field chlorophyll-a (P/salinity)

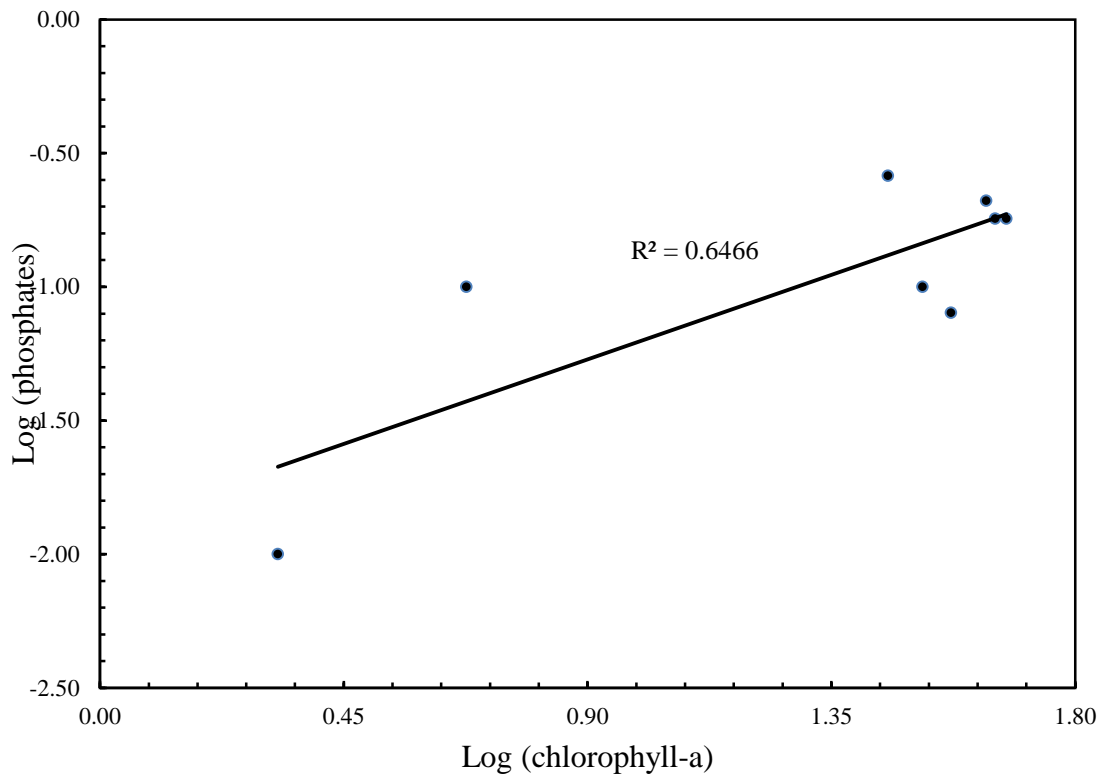


Figure 19: Correlation between eutrophication indicators and field chlorophyll-a (phosphates)

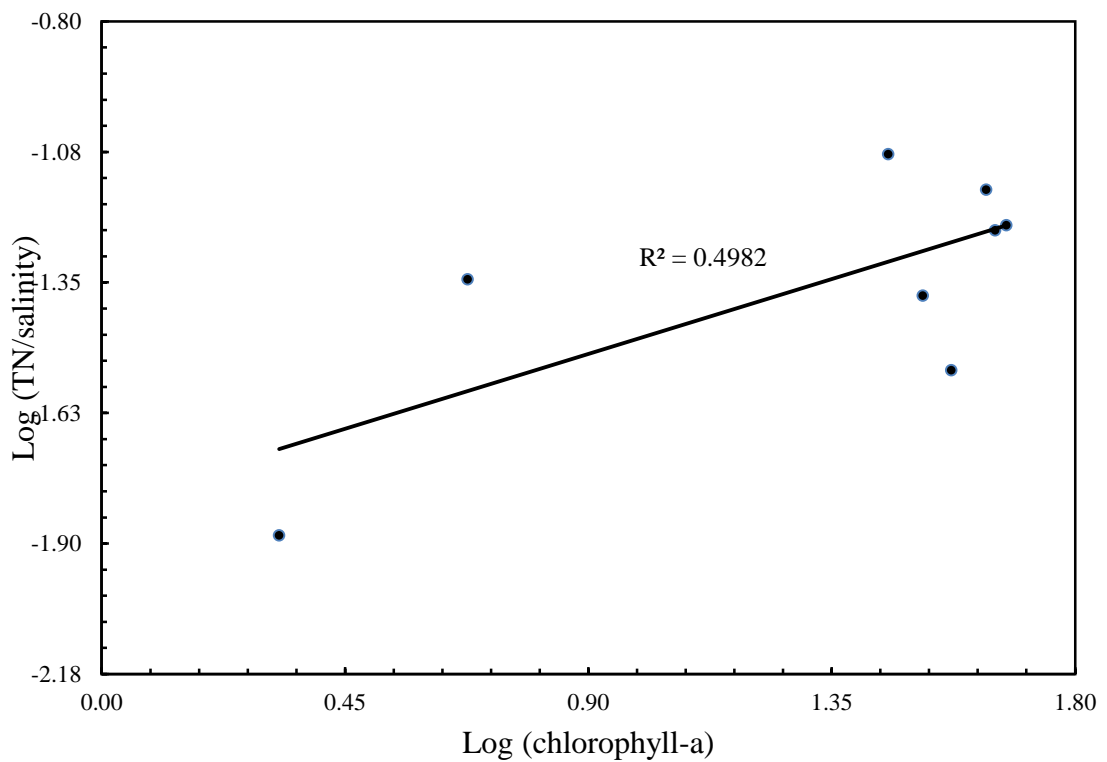


Figure 20: Correlation between eutrophication indicators and field chlorophyll-a (TN/salinity)

The following model, which has produced the highest R-squared value, was selected for further analysis:

$$\log \frac{\text{TN}}{\text{P}} = -0.388 \times \log(\text{chl} - \text{a}) + 1.6982 \quad (13)$$

where TN, P, and chl-a are total nitrogen, phosphates, and chlorophyll-a; respectively.

The values of the in-situ and modeled total nitrogen-phosphorus ratio in the creek are illustrated in Table 16, and the relationship is plotted in Figure 21. This relationship produced an R-squared value of about 0.80, which indicates that the model is very good in predicting the ratio of total nitrogen-phosphates in quarter 2, 2012 given the in-situ chlorophyll-a data. This high correlation is similar to that obtained in a study carried out by Liu et al. to understand the influence of water chemistry on chlorophyll-a [49]. However, the correlation obtained here is stronger than that obtained in two similar studies [45, 46].

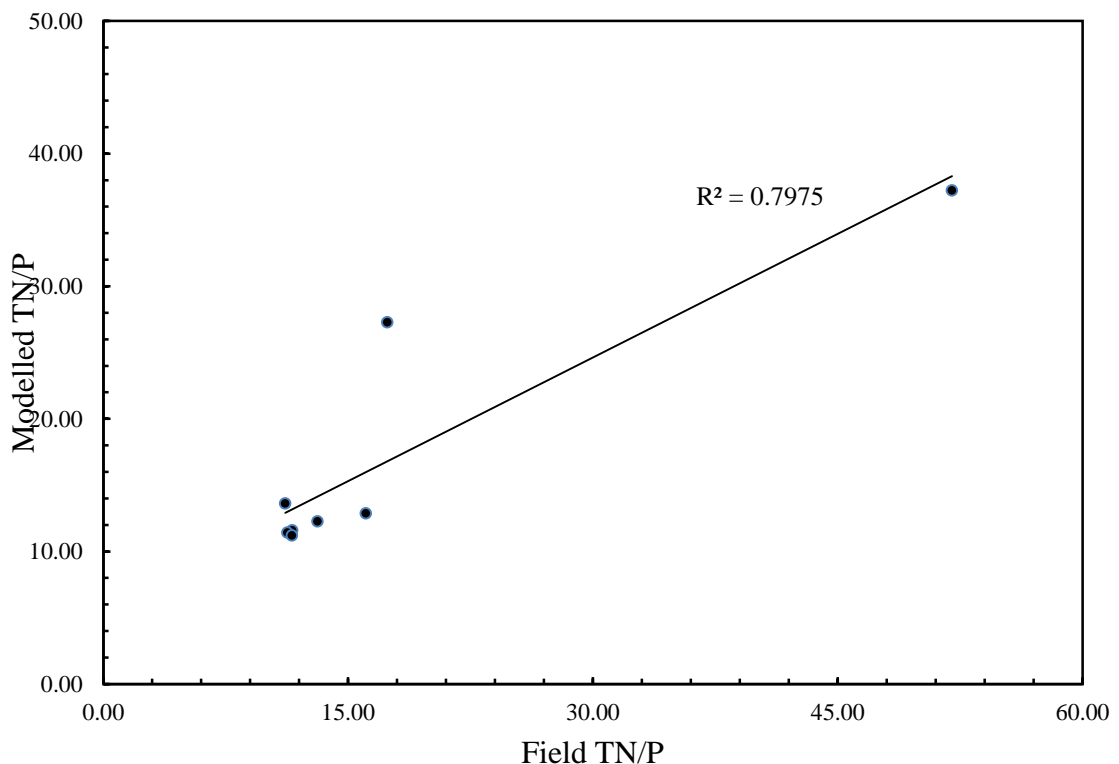


Figure 21: Correlation between field and modelled TN-P ratio

4.4 Correlation between Spectral chlorophyll-a and Eutrophication Indicators

The model of Equation 13 was applied to the spectral chlorophyll-a map presented in Figure 15 which was developed according to Equation 12. ERDAS Imagine 2011 was used to calculate TN/P values for each pixel located in Dubai Creek as shown in Figure 7. The map was then color-coded using ArcMap 9.3 and is shown in Figure 22. A summary of the various computed values necessary for the modeling efforts in this study are summarized in Table 17. A conversion from the TN/P values used in the map to their corresponding spectral chlorophyll-a values is provided in Table 18.

There are many observations to be made from the map, which can be summarized as follows:

- (a) The TN/P ratio in the northern half of the creek is mostly in the range of 15-40, which matches the chlorophyll-a concentrations shown in Figure 15.
- (b) Concentrations of less than 10 $\mu\text{g/l}$ are observed in this same part of the creek indicated above, which corresponds to the high TN/P ratios at the creek edges in Figure 22.
- (c) The ratio in the lagoon part of the creek is mostly between 11 and 15 while it's a little bit less than that around some of the edges of the lagoon. This goes as well in accordance with the chlorophyll-a concentrations found in that part of the creek where they are mainly higher than 30 $\mu\text{g/l}$.
- (d) It's important to note that around the edges of the lagoon the TN/P ratio is a little bit lower than the middle of the lagoon which corresponds to higher chlorophyll-a concentrations. This is because the Al Awir sewage treatment plant is discharging its effluent in this area, which also suffers from poor flushing.

The plot of the log of spectral chlorophyll-a against the log of field TN/P shown in Figure 23 produced an R-squared value of about 95%. This is rather a higher correlation compared to that of the log of field chlorophyll-a, which produced an R-squared value of about 78%. The reason for such an increase could be the two outliers that correspond to the creek mouth and wharfage stations, which can be seen in Figure 16. Due to the difference between the values of the spectral and in-situ chlorophyll-a values at the monitoring stations, these two outliers happened to be closer to the regression line in Figure 23.

Table 16: Comparison between field and modelled TN/P values

Stations	Field chl-a mg/l	LOG (TN/P) (modelled)	TN/P modelled	LOG (field TN/P)	Field TN/P	% Error
Creek Mouth	2.13	1.57	37.22	1.72	52	28.42
Abra	33	1.11	12.86	1.21	16.1	20.15
Wharfage	4.75	1.44	27.27	1.24	17.4	56.71
Floating Bridge	28.5	1.13	13.61	1.05	11.15	22.02
Dubai Festival City	43.3	1.06	11.57	1.06	11.57	0.01
STP Outfall	44.9	1.06	11.4	1.05	11.28	1.11
Jaddaf	47.1	1.05	11.19	1.06	11.56	3.13
Sanctuary	37.3	1.09	12.26	1.12	13.13	6.57

Table 17: Summarization of the modelling steps

Stations	CB	NIR1	NIR2	(CB+IR1)/IR2	Spectral chl-a mg/l	LOG (Spectral TN/P)	LOG (field TN/P)	Spectral TN/P	Field TN/P
Creek Mouth	0.02126	0.03865	0.03372	1.777	2.242	1.562	1.716	36.486	52
Abra	0.02427	0.05428	0.04222	1.86	22.611	1.173	1.207	14.884	16.1
Wharfage	0.02014	0.04972	0.03833	1.823	13.399	1.261	1.241	18.234	17.4
Floating Bridge	0.02652	0.05819	0.04435	1.91	34.653	1.101	1.047	12.612	11.153
Dubai Festival City	0.0299	0.06535	0.04966	1.918	36.599	1.092	1.063	12.347	11.571
STP Outfall	0.03816	0.07577	0.05922	1.924	38.009	1.085	1.052	12.168	11.278
Jaddaf	0.0269	0.05754	0.04293	1.967	48.48	1.044	1.063	11.071	11.556
Sanctuary	0.02577	0.04907	0.03833	1.953	44.979	1.057	1.118	11.398	13.125

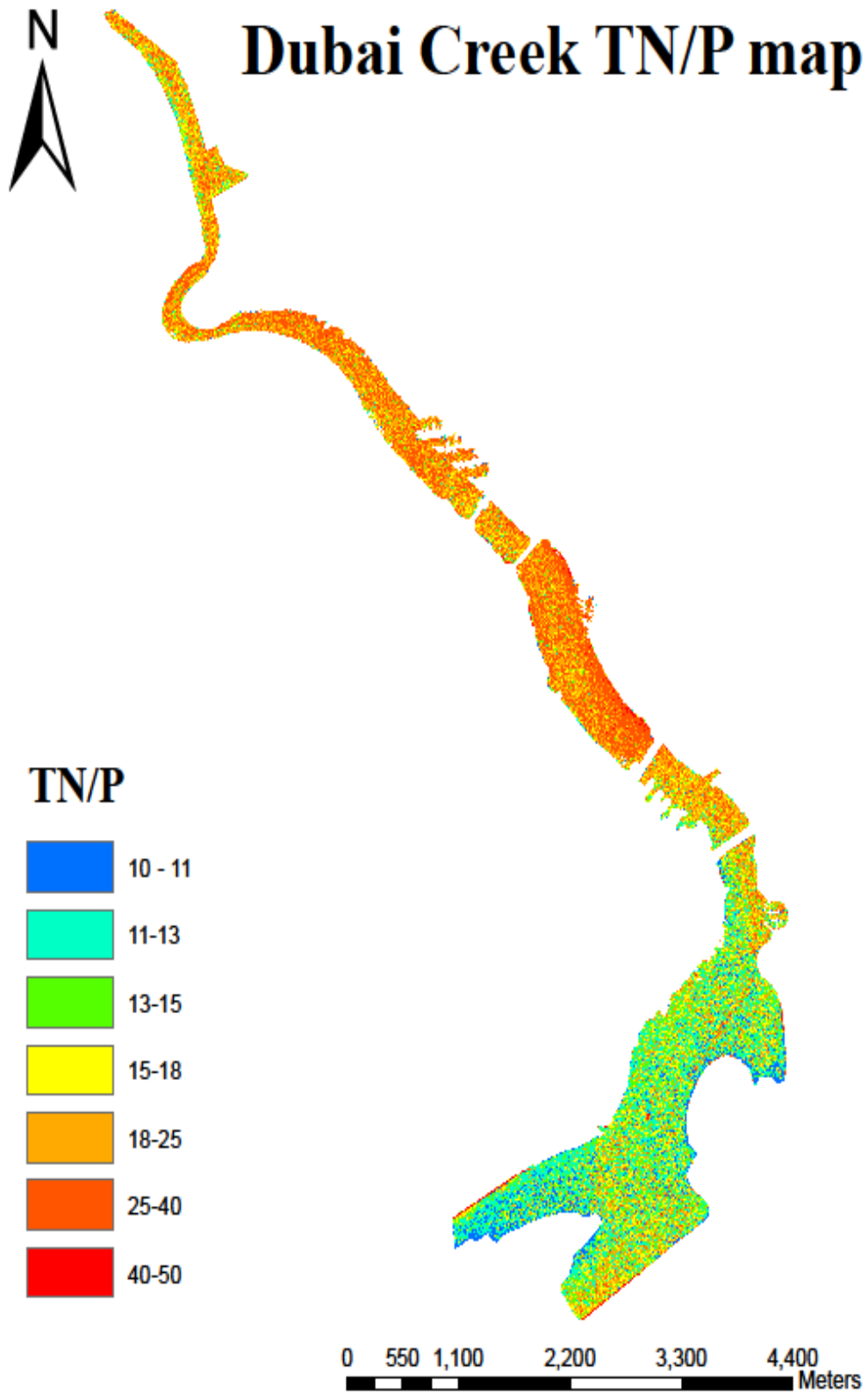


Figure 22: Dubai Creek TN/P map

Table 18: Spectral TN/P and corresponding spectral chlorophyll-a values

Point	Spectral TN/P	Corresponding spectral chl-a $\mu\text{g/l}$
1	10	63
2	11	49.29
3	13	32.05
4	15	22.16
5	18	13.85
6	25	5.94
7	40	1.77
8	50	1

Similarly, when examining the regression model of the relationship between spectral and field TN/P ratios shown in Figure 24 and comparing it to the model of Figure 21, it can be seen that the outlier at the Wharfage station is the cause of the difference between the R-squared values of the two models.

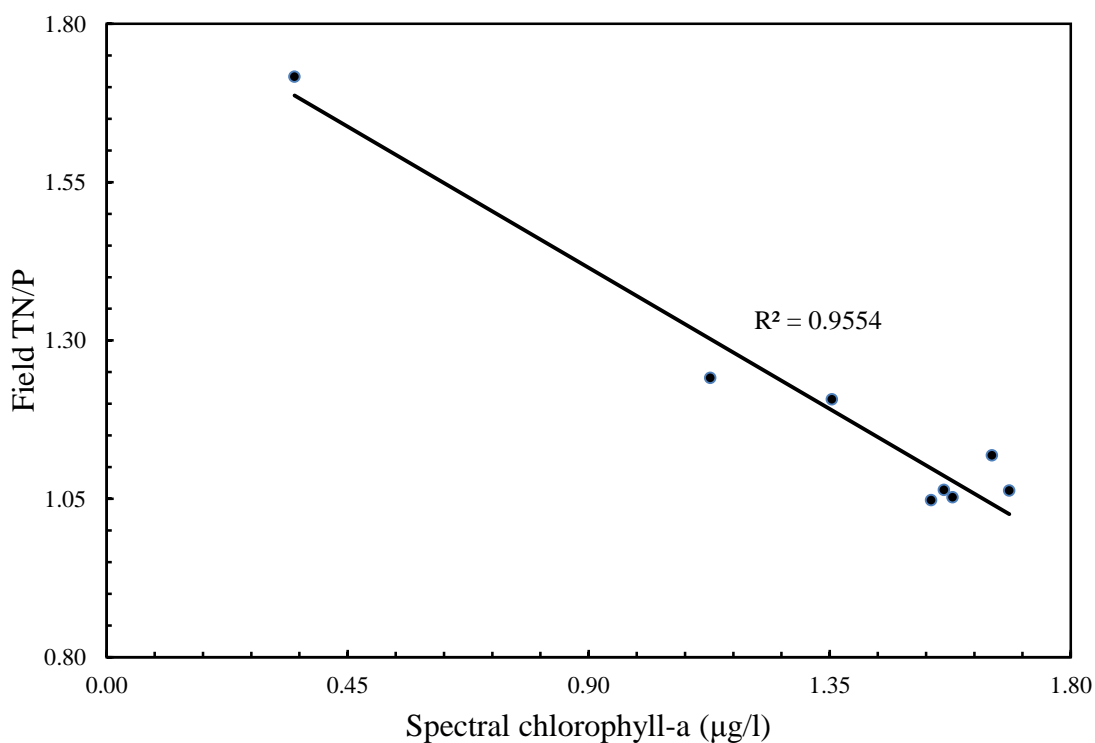


Figure 23: Correlation between spectral chlorophyll-a and field TN/P

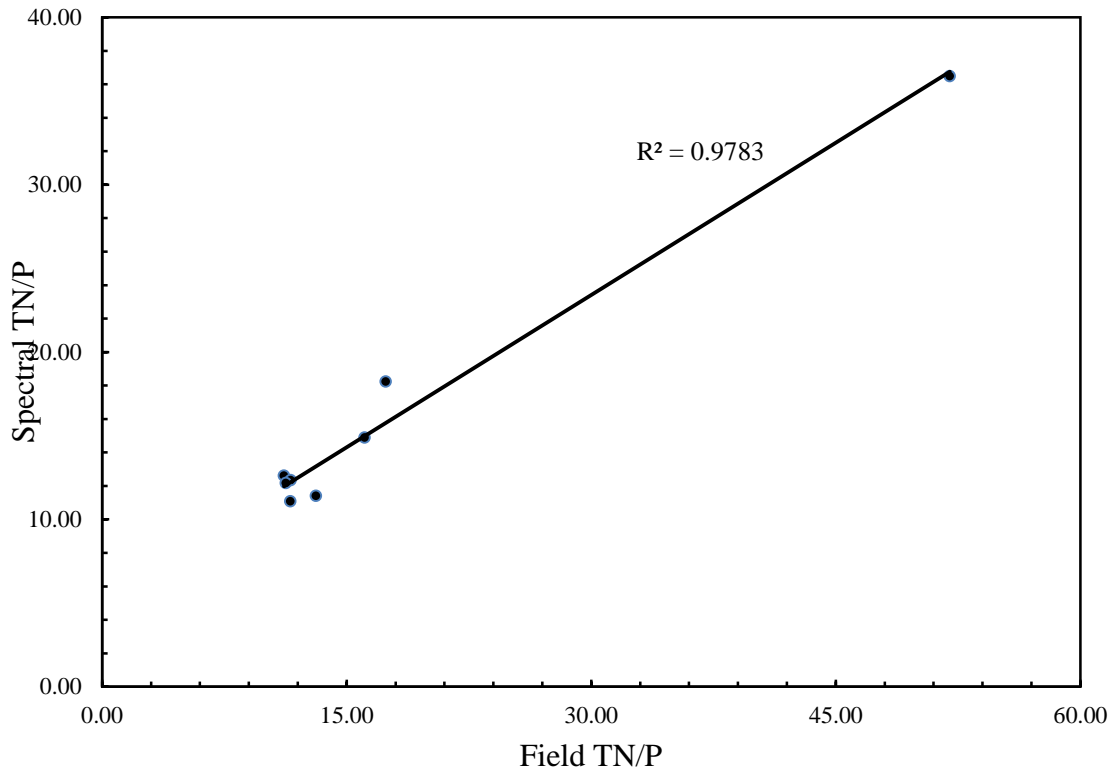


Figure 24: Correlation between spectral and field TN-P ratios

5 Conclusions and Future Work

5.1 Conclusions

Corrected high resolution imagery of WorldView-2 for geometric, radiometric, and atmospheric errors was utilized in this study to map chlorophyll-a in the Dubai Creek on the 24th of July, 2012. The developed model can predict chlorophyll-a with an R-squared value of about 82%. The model combines the two near infrared bands of WorldView-2 imagery. The model shows that most parts of the Creek have chlorophyll-a concentrations that were well above the limits allowed by OECD, especially the lagoon part of the creek. These high concentrations were attributed to the major source of pollution in the creek, the disposal of effluents from the Al Awir sewage treatment plant in the lagoon part of the creek.

Another model was developed using regression analysis to estimate some of the eutrophication indicators from chlorophyll-a values. The model with the highest correlation was that of the total nitrogen-phosphate ratio and chlorophyll-a. This was expected as these nutrients play an important role in the eutrophication process. A comparison of actual TN/P values with predicted ones showed a high correlation coefficient (R-squared = 79%). This model was used with the spectral chlorophyll-a values to estimate the pixel-based corresponding TN/P values in the creek. The produced TN/P map of the creek provided expected results when combined with the chlorophyll-a distribution. Lower TN/P ratios and higher chlorophyll-a concentrations were found in the lagoon part compared to the upper half of the creek because of the anthropogenic activities and poor flushing in this area. In conclusion, the two models developed in this study were useful in robustly relating the spectral characteristics of the water column to its chlorophyll-a and nutrient content.

5.2 Future Work

There were two main limitations faced in this study. One is the small number of monitoring stations. The other one is the data being provided in quarter averages rather than daily averages. Conducting this study without these limitations would provide beneficial for future studies.

References

- [1] B. Nas, H. Karabork, S. Ekercin, A. Berkay, "Mapping of chlorophyll-a through in-situ measurements and Terra ASTER satellite data," *Environmental Monitoring and Assessment*, Vol. 157, pp. 375-382, Oct. 2009.
- [2] D. Blondeau-Patissier, J. Gowe, A. Dekker, S. Phinn, V. Brando, "A review of ocean color remote sensing methods and statistical techniques for the detection, mapping and analysis of phytoplankton blooms in coastal and open oceans," *Progress in oceanography*, Vol. 123, pp. 123-144, Apr. 2014.
- [3] M. Richlen, S. Morton, E. Jamali, A. Rajan, D. Anderson, "The catastrophic 2008–2009 red tide in the Arabian gulf region, with observations on the identification and phylogeny of the fish-killing dinoflagellate *Cochlodinium polykrikoides*," *Harmful Algae*, Vol. 9, pp. 163-172, Feb. 2010.
- [4] T. Ali, M. Mortula, S. Atabay, "Study of water quality in Dubai Creek using DubaiSat-1 multispectral imagery," *Communications in Computer and Information Science*, Vol. 398, pp. 200-210, Nov. 2013.
- [5] J. Zhao, H. Ghedira, "Monitoring red tide with satellite imagery and numerical models: A case study in the Arabian Gulf," *Marine Pollution Bulletin*, Vol. 97, pp. 305-313, Feb. 2014.
- [6] M. Matthews, "A current review of empirical procedures of remote sensing in inland and near-coastal transitional waters," *International Journal of Remote Sensing*, Vol. 32, pp. 6855-6899, Aug. 2011.
- [7] S. Jain, V. Singh, *Water Resources Systems Planning and Management*, Manhattan: Elsevier Science B.V., 2003, pp. 1-12.
- [8] K. Loague, D. Corwin, *Point and Nonpoint Source Pollution*, New York: John Wiley & Sons, 2005, pp. 1-20.
- [9] K. Sellner, G. Doucette, G. Kirkpatrick, "Harmful algal blooms: causes, impacts and detection," *Journal of Industrial Microbiology Biotechnology*, Vol. 30, pp. 383-406, Jul. 2003.
- [10] K. Victor, "Remote sensing of algal blooms: an overview with case studies," *Journal of Coastal Research*, Vol. 28, pp. 34-43, Jan. 2012.
- [11] T. Davis, D. Berry, G. Boyer, C. Gobler, "The effects of temperature and nutrients on the growth and dynamics of toxic and non-toxic strains of *Microcystis* during cyanobacteria blooms," *Harmful Algae*, Vol. 8, pp. 715-725, Jun. 2009.
- [12] T. D. Jickells, "Nutrient biogeochemistry of the coastal zone," *Science*, Vol. 281, pp. 217-21, Jul. 1998.

- [13] R. Miller, B. McKee, "Using MODIS Terra 250 m imagery to map concentrations of total suspended matter in coastal waters," *Remote Sensing of Environment*, Vol. 93, pp. 259-266, Oct. 2004.
- [14] M. Krom, B. Herut, R. Mantoura, "Nutrient budget for the Eastern Mediterranean: Implications for phosphorus limitation," *Limnology and Oceanography*, Vol. 49, pp. 1582-1592, May. 2004.
- [15] R. Domingues, T. Anselmoa, A. Barbosaa, U. Sommer, H. Galvãoa, "Nutrient limitation of phytoplankton growth in the freshwater tidal zone of a turbid, Mediterranean estuary," *Coastal and Shelf Science*, Vol. 91, pp. 282-297, Jan. 2011.
- [16] Y. Ahn, P. Shanmugam, J. Ryu, J. Jeong, "Satellite detection of harmful algal bloom occurrences in Korean waters," *Harmful Algae*, Vol. 5, pp. 213-231, Mar. 2006.
- [17] P. Shanmugam, Y. Ahn, P. Ram, "SeaWiFS sensing of hazardous algal blooms and their underlying mechanisms in shelf-slope waters of the Northwest Pacific during summer," *Remote Sensing of Environment*, Vol. 112, pp. 3248-3270, Jul. 2008.
- [18] M. Tomlinson, T. Wynne, R. Stumpf, "An evaluation of remote sensing techniques for enhanced detection of the toxic dinoflagellate, *Karenia brevis*," *Remote Sensing of Environment*, Vol. 113, pp. 598-609, Mar. 2009.
- [19] R. Schowengerdt, *Remote Sensing: Models and Methods for Image Processing*, Burlington: Academic Press, 2007, pp 1-44.
- [20] N. Levin, "Electromagnetic radiation," *Fundamentals of Remote Sensing*, Trieste, Italy: International Maritime Academy, 1999 pp. 9-15.
- [21] J. Chen, M. Zhang, T. Cui, Z. Wen, "A review of some important technical problems in respect of satellite remote sensing of chlorophyll-a concentration in coastal waters," *IEEE Journal of Selected Topics in Applied Earth Observations and Remote Sensing*, Vol. 6, pp. 2275-2289, Oct. 2013.
- [22] S. Liang, *Quantitative remote sensing of land surfaces*, Manhattan: John Wiley and Sons, Inc., 2004 pp 1-24.
- [23] P. Chavez, "Image-based atmospheric correction: revisited and improved," *Photogrammetric Engineering and Remote Sensing*, Vol. 62, pp. 1025-1036, Sep. 1996.
- [24] J. Martin, F. Eugenio, J. Marcello, A. Medina, J. Bermejo, M. Arbelo, "Atmospheric correction models for high resolution WorldView-2 multispectral imagery: a case study in Canary Islands, Spain," *Remote Sensing of Clouds and the Atmosphere*, Vol. 8534, pp. 10, 2012.

- [25] G. Smith, E. Milton, "The use of the empirical line method to calibrate remotely sensed data to reflectance," *International Journal of Remote Sensing*, Vol. 20, pp. 2653-2662, Sep. 1999.
- [26] E. Karpouzi, T. Malthus, "The empirical line method for the atmospheric correction of IKONOS imagery," *International Journal of Remote Sensing*, Vol. 24, pp. 1143-1150, Mar. 2003.
- [27] MODIS specifications. (n.d.), NASA MODIS web, [Online], Available: <http://modis.gsfc.nasa.gov/about/specifications.php>, Accessed Jan. 24, 2015.
- [28] G. Dial, H. Bowen, F. Gerlach, J. Grodecki, R. Oleszczuk, "IKONOS satellite, imagery, and products," *Remote Sensing of Environment*, Vol. 88, pp. 23-36, Aug. 2003.
- [29] SPOT-6 Satellite Sensor, (n.d.), Satellite imaging corporation, [Online], Available: <http://www.satimagingcorp.com/satellite-sensors/spot-6.html>, Accessed Jan. 24, 2015.
- [30] An Overview of SeaWiFS and the SeaStar Spacecraft. (n.d.). NASA earth observatory. [Online]. Available: <http://oceancolor.gsfc.nasa.gov/SeaWiFS/SEASTAR/SPACECRAFT.html>, Accessed Mar. 30, 2014.
- [31] MERIS Instrument. (n.d.), ESA, [Online], Available: <https://earth.esa.int/web/guest/missions/esa-operational-eo-missions/envisat/instruments/meris>, Accessed Mar. 31, 2014.
- [32] Landsat 8 Instruments, (n.d.), USGS. [Online], Available <http://landsat.usgs.gov/landsat8.php>, Accessed Mar. 31, 2014.
- [33] G. Dial, H. Bowen, F. Gerlach, J. Grodecki, R. Oleszczuk, (2010, Mar.). The benefits of the 8 spectral bands of worldview-2. [Online]. Available: http://www.army.mil/article/70358/Nano_technology_marches_on/, Accessed Jan. 24, 2015.
- [34] Z. Lee, (2006). IOCCG report number 5. [Online]. Available: http://www.army.mil/article/70358/Nano_technology_marches_on/, Accessed Jan. 24, 2015.
- [35] H. Duan, R. Ma, "Validation of MERIS case-2 water products in Lake Taihu, China," *GIScience & Remote Sensing*, Vol. 49, pp. 873-894, May. 2012.
- [36] M. Defoin-Platel, M. Chami "How ambiguous is the inverse problem of ocean color in coastal waters?," *Journal of Geophysical Research: Oceans*, Vol. 112, pp. 1978-2012, Mar. 2007.
- [37] K. Carder, F. Chena, J. Cannizzaro, J. Campbell, B. Mitchell, "Performance of the MODIS semi-analytical ocean color algorithm for chlorophyll-a," *Advances in Space Research*, Vol. 33, pp. 1152-1159, Apr. 2004.

- [38] H. Duan, Y. Zhang, B. Zhang, K. Song, Z. Wang, "Assessment of chlorophyll-a concentration and trophic state for Lake Chagan using Landsat TM and field spectral data," *Environmental Monitoring and Assessment*, Vol. 129, pp. 295-308, Jun. 2006.
- [39] H. Dierssen, "Perspective on empirical approaches for ocean color remote sensing of chlorophyll in a changing climate," *Advances in Space Research*, Vol. 107, pp. 17073-17078, Oct. 2010.
- [40] P. Brivio, C. Giardino, E. Zilioli, "Determination of chlorophyll concentration changes in Lake Garda using an image-based radiative transfer code for Landsat TM images," *International Journal of Remote Sensing*, Vol. 22, pp. 487-502, Jan. 2001.
- [41] L. Han, K. Jordan, "Estimating and mapping chlorophyll-a concentration in Pensacola Bay, Florida using Landsat ETM+ data," *International Journal of Remote Sensing*, Vol. 26, pp. 5245-5254, Dec. 2005.
- [42] C. Ormeci, E. Sertel, O. Sarikaya, "Determination of chlorophyll-a amount in Golden Horn, Istanbul, Turkey using IKONOS and in-situ data," *Environmental Monitoring and Assessment*, Vol. 155, pp. 83-90, Aug. 2009.
- [43] T. Upkide, C. Comp, (2010, Nov. 1). Radiometric Use of WorldView-2 Imagery. [Online]. Available: https://www.digitalglobe.com/sites/default/files/Radiometric_Use_of_WorldView-2_Imagery%20%281%29.pdf, Accessed Jan. 24, 2015.
- [44] S. Nixon, "Coastal marine eutrophication: A definition, social causes, and future concerns," *Ophelia*, Vol. 41, pp. 199-219, Feb. 1995.
- [45] L. Hakanson, J. Eklund, "Relationships between chlorophyll, salinity, phosphorus, and nitrogen in lakes and marine areas," *Journal of Coastal Research*, Vol. 26, pp. 412-423, Jan. 2010.
- [46] E. Nieuwenhuys, J. Jones, "Phosphorus-chlorophyll relationship in temperate streams and its variation with stream catchment area," *Journal of Fish and Aquatic Sciences*, Vol. 53, pp. 99-105, Jan. 1996.
- [47] A. Mahiny, B. Turner, "A comparison of four common atmospheric correction methods," *Photogrammetric Engineering and Remote Sensing*, Vol. 73, pp. 361-368, Apr. 2007.
- [48] H. Caspers, "Eutrophication of waters, monitoring, assessment and control," *Organization for Economic Cooperation and Development*, Vol. 69, pp. 200, Jun. 1982.
- [49] Y. Liu, H. Guo, P. Yang, "Exploring the influence of lake water chemistry on chlorophyll-a: a multi-iterative statistical model analysis," *Ecological Modeling*, Vol. 221, pp. 681-688, Jan. 2010.

Appendix A: Earth-Sun Distance Calculation [43]:

The acquisition date and time of the scene is (2012-07-24) at (7:23:39.603905).

Acquired from the metadata file:

(earliestAcqTime = 2012-07-24T07:23:39.603905Z)

$$d_{ES} = 1.00014 - 0.01671 * \cos(g) - 0.00014 * \cos(2g)$$

d_{ES} value should be between 0.983 and 1.017 AU.

$$g = 357.529 + 0.98560028 * D$$

$D = JD - 2451545$ where JD is the Julian day of the scene.

$$JD = \text{int}(365.25(\text{year} + 4716)) + \text{int}(30.6001(\text{month} + 1)) + \text{day} + (\text{UT}/24) + B - 1524.5$$

Where: int is an integer number (i.e. ignore the numbers after the decimal)

Year, month, and day are those of the acquisition time of the scene.

$$B = 2 - A + \text{int}(A/4) \text{ and,}$$

$$A = \text{int}(\text{year}/100)$$

UT is the universal time of the scene and is calculated as follows:

$UT = \text{hh} + (\text{mm}/60) + (\text{ss}.\text{dddddd}/3600)$ where h, m, s, and d are the hour, minute, second, and decimals of the second of the scene acquisition time.

$$UT = 7 + (23/60) + (39.603905/3600) = 7.394334418$$

$$A = \text{int}(2012/100) = 20.12 \text{ (ignoring the decimals)} = (20)$$

$$B = 2 - 20 + \text{int}(20/4) = -13$$

$$JD = \text{int}(365.25(2012 + 4716)) + \text{int}(30.6001(7 + 1)) + 24 + (7.394334418/24) - 13 - 1524.5$$

$$JD = 2456132.808097267$$

$$D = 2456132.808097267 - 2451545 = 4587.808097$$

$$g = 357.529 + 0.98560028 * (4587.808097)$$

$$g = 4879.273945$$

$$d_{ES} = 1.00014 - 0.01671 * \cos(4879.273945) - 0.00014 * \cos(2 * 4879.273945)$$

$$d_{ES} = 1.01580393 \text{ AU which is between } (0.983 \text{ and } 1.017)$$

$$\text{Therefore, } d_{ES}^2 = 1.01580393^2 = 1.031857624$$

Appendix B: Solar Zenith Angle Calculation (θ_s) [43]:

$$\theta_s = 90.0 - \text{sunEL}$$

Where sunEL is the sun elevation at the acquisition time of the scene.

Acquired from the metadata file:

$$(\text{meanSunEl} = 74.8).$$

$$\theta_s = 90.0 - 74.8 = 15.2$$

Conversion of θ_s from degrees to radian since ERDAS Imagine processing uses radian values.

$$\theta_s(\text{radian}) = \theta_s(\text{degrees}) * \pi / 180 = 15.2 * \pi / 180 = 0.265290046$$

Appendix C: Conversion from Digital Numbers to Top-of-Atmosphere Radiance to Ground-Leaving Reflectance [Equation1-Equation10]:

Table A.1: Digital numbers corresponding to stations locations

DUBAI CREEK	Digital numbers							
	Station Name	coastal	blue	green	yellow	red	red edge	NIR1
Creek mouth	446	270	321	292	131	195	102	148
Abra	454	277	325	315	145	215	126	172
Wharfage	443	272	320	302	146	222	119	161
Floating Bridge	460	286	329	333	145	227	132	178
Dubai Festival City	469	289	361	336	163	231	143	193

STP Outfall	491	316	386	384	183	282	159	220
Al Jaddaf	461	285	342	327	152	227	131	174
Sanctuary	458	281	327	307	148	209	118	161

Table A.2: Top-of-atmosphere radiance corresponding to stations locations

DUBAI CREEK	Top-of-atmosphere radiance							
	Station Name	coastal	blue	green	yellow	red	red edge	NIR1
Creek mouth	87.650	88.686	69.509	53.175	42.261	30.084	21.151	13.436
Abra	89.223	90.985	70.375	57.363	46.777	33.169	26.128	15.615
Wharfage	87.061	89.343	69.293	54.996	47.099	34.249	24.676	14.616
Floating Bridge	90.402	93.941	71.241	60.641	46.777	35.021	27.372	16.16
Dubai Festival City	92.170	94.927	78.171	61.187	52.584	35.638	29.653	17.522
STP Outfall	96.494	103.795	83.584	69.928	59.036	43.507	32.971	19.973
Al Jaddaf	90.598	93.613	74.056	59.548	49.035	35.021	27.165	15.797
Sanctuary	90.009	92.299	70.808	55.906	47.745	32.244	24.469	14.616

Table A.3: Ground-leaving reflectance corresponding to stations locations

DUBAI CREEK	Ground-leaving reflectance							
	Station Name	coastal	blue	green	yellow	red	red edge	NIR1
Creek mouth	0.0194	0.0273	0.0312	0.0357	0.0371	0.0366	0.0386	0.0337
Abra	0.0224	0.0312	0.0327	0.0438	0.0468	0.0443	0.0543	0.0422
Wharfage	0.0183	0.0284	0.0308	0.0392	0.0475	0.0471	0.0497	0.0383
Floating Bridge	0.0246	0.0363	0.0343	0.0501	0.0468	0.0490	0.0582	0.0444
Dubai Festival City	0.0280	0.0379	0.0468	0.0512	0.0593	0.0505	0.0653	0.0497
STP Outfall	0.0363	0.053	0.0566	0.0681	0.0732	0.0702	0.0758	0.0592
Al Jaddaf	0.0250	0.0357	0.0394	0.05	0.0517	0.049	0.0575	0.0429
Sanctuary	0.0239	0.0335	0.0335	0.0409	0.0489	0.0421	0.0491	0.0383

Verification of accuracy of computed values through randomly selected points:

Table A.4: Randomly selected DN values and their conversion parameters

Point	Station	Band	Digital Number	K_{band} (from table 8)	$\Delta\lambda_{band}$ (from table 8)
1	Abra	Blue	277	$1.783568e^{-2}$	$5.43e^{-2}$
2	Floating Bridge	NIR2	178	$9.042234e^{-3}$	$9.96e^{-2}$
3	STP Outfall	Red	183	$1.851735e^{-2}$	$5.74e^{-2}$

$$L_{\lambda_{pixel,band}} = (K_{band} * q_{pixel,band}) / \Delta\lambda_{band}$$

Point 1: $L_{\lambda_{pixel,band}} = ((1.783568e^{-2}) * (277)) / (5.43e^{-2}) = 90.985$

Point 2: $L_{\lambda_{pixel,band}} = ((9.042234e^{-3}) * (178)) / (9.96e^{-2}) = 16.160$

Point 3: $L_{\lambda_{pixel,band}} = ((1.851735e^{-2}) * (183)) / (5.74e^{-2}) = 59.036$

These values are the same as the values marked with Red in (Table A.2).

Table A.5: Randomly selected radiance values and their conversion parameters

Point	Station	Band	Radiance	Haze radiance (table 10)	Spectral irradiance (table 9)
1	Creek Mouth	Red-Edge	30.084	19.44	1342.0695
2	Wharfage	Green	69.293	12.03	1856.4104
3	Al Jaddaf	NIR1	27.165	57.82	1069.7302

Other required values:

$$d_{ES}^2 = 1.031857624 \text{ and } \text{COS}(\theta_s) \text{ (Radian)} = 0.265290046$$

$$\rho_{\lambda_{pixel,band}} = (((L_{\lambda_{pixel,band}} - L_{\lambda_{haze,band}}) * d_{ES}^2 * \pi) / (E_{sun\lambda,band} * \text{cos}(\theta_s))) + 0.01$$

Point 1: $\rho_{\lambda_{pixel,band}} = (((30.084 - 19.44) * 1.031857624 * \pi) / (1342.0695 * \text{COS}(0.26590046))) + 0.01 = 0.0366$

Point 2: $\rho_{\lambda_{pixel,band}} = (((69.293 - 57.82) * 1.031857624 * \pi) / (1856.4104 * \text{COS}(0.26590046))) + 0.01 = 0.0308$

Point 3: $\rho_{\lambda_{\text{pixel,band}}} = (((27.165 - 12.03) * 1.031857624 * \pi) / (1069.7302 * \cos(0.26590046))) + 0.01 = 0.0575$

These values are the same as the values marked with Blue in (Table A.3).

Vita

Abdallah Bachir was born in 2nd of September, 1987, in Dubai, United Arab Emirates. He received his high school certificate from Al-Rashediya Secondary School, Ajman. He joined the American University of Sharjah in 2006 and received a Bachelor's degree of science in civil engineering in 2010. Then he started his Master's degree studies in September, 2011. During his Master's degree studies he worked as a graduate teaching assistant and graduate research assistant. He assisted in lab sessions, was involved in research, and performed classroom tasks such as grading and lecturing.